



저작자표시-비영리-변경금지 2.0 대한민국

이용자는 아래의 조건을 따르는 경우에 한하여 자유롭게

- 이 저작물을 복제, 배포, 전송, 전시, 공연 및 방송할 수 있습니다.

다음과 같은 조건을 따라야 합니다:



저작자표시. 귀하는 원저작자를 표시하여야 합니다.



비영리. 귀하는 이 저작물을 영리 목적으로 이용할 수 없습니다.



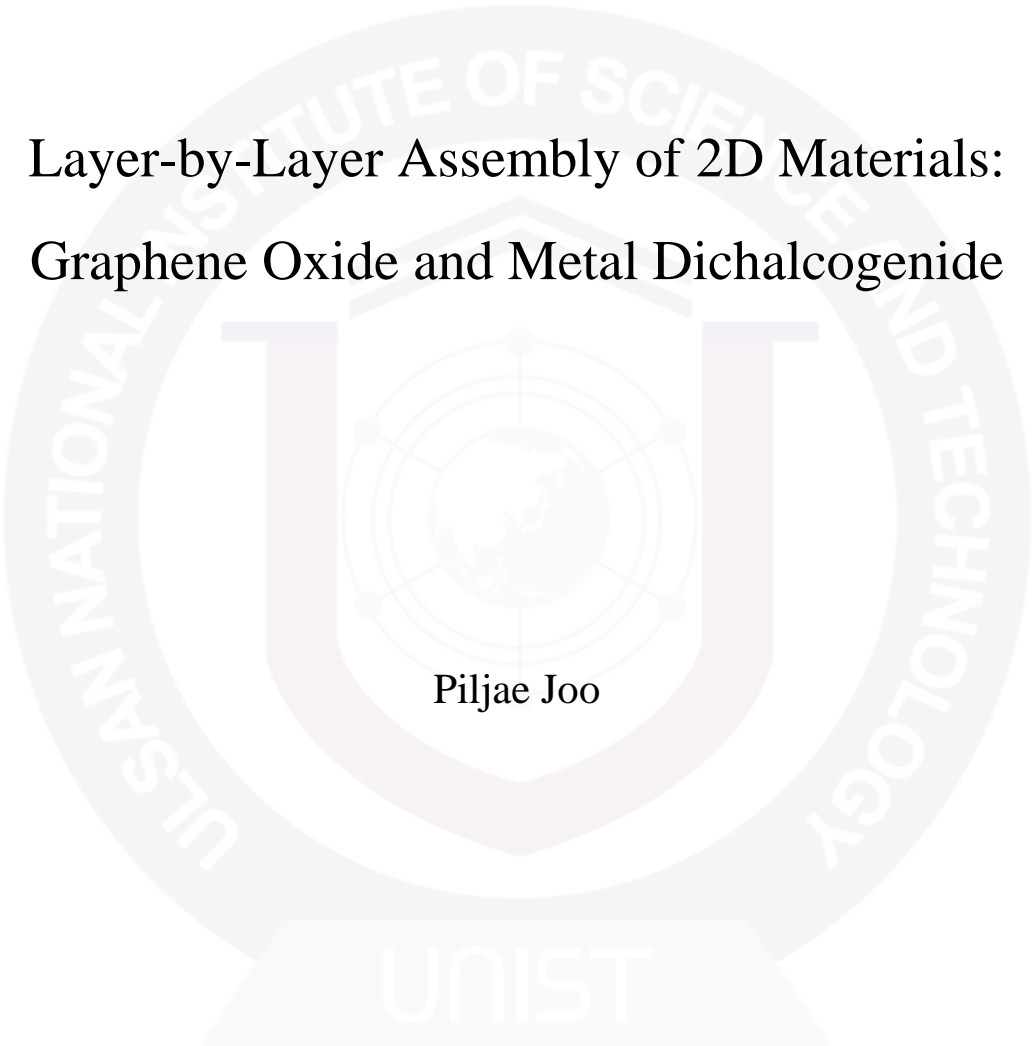
변경금지. 귀하는 이 저작물을 개작, 변형 또는 가공할 수 없습니다.

- 귀하는, 이 저작물의 재이용이나 배포의 경우, 이 저작물에 적용된 이용허락조건을 명확하게 나타내어야 합니다.
- 저작권자로부터 별도의 허가를 받으면 이러한 조건들은 적용되지 않습니다.

저작권법에 따른 이용자의 권리는 위의 내용에 의하여 영향을 받지 않습니다.

이것은 [이용허락규약\(Legal Code\)](#)을 이해하기 쉽게 요약한 것입니다.

[Disclaimer](#)

The background features a large, light gray watermark of the UNIST logo. It consists of a circular emblem with the text 'UNIST NATIONAL INSTITUTE OF SCIENCE AND TECHNOLOGY' around the perimeter. Inside the circle is a stylized 'U' shape containing a globe and a molecular structure. Below the circle is a trapezoidal base with the word 'UNIST' written on it.

Layer-by-Layer Assembly of 2D Materials:
Graphene Oxide and Metal Dichalcogenide

Piljae Joo

Energy Conversion and Storage Program
Interdisciplinary School of Green Energy
Graduate School of UNIST

2013

Layer-by-Layer Assembly of 2D Materials: Graphene Oxide and Metal Dichalcogenide

Piljae Joo

Energy Conversion and Storage Program
Interdisciplinary School of Green Energy
Graduate School of UNIST

Layer-by-Layer Assembly of 2D Materials: Graphene Oxide and Metal Dichalcogenide

A thesis

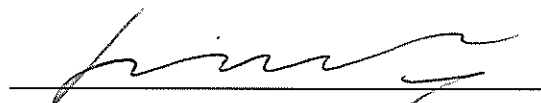
Submitted to the Interdisciplinary School of Green Energy
and the Graduate School of UNIST

In partial fulfillment of the
Requirements for the degree of
Master of Science

Piljae Joo

02. 06. 2013 [Month/Day/Year of submission]

Approved by



Major Advisor

Byeong-Su Kim

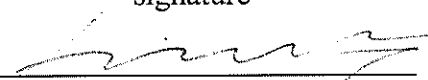
Layer-by-Layer Assembly of 2D Materials: Graphene Oxide and Metal Dichalcogenide

Piljae Joo

This certifies that the thesis of Piljae Joo is approved.

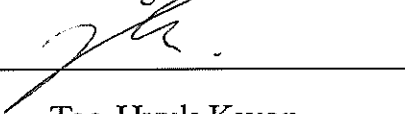
02. 06. 2013 [Month/Day/Year of submission]

signature



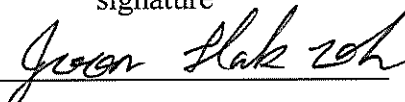
Byeong-Su Kim

signature



Tae-Hyuk Kwon

signature



Joon Hak Oh

Abstract

Layer-by-Layer Assembly of 2D Materials: Graphene Oxide and 2D Metal Dichalcogenides, 2013, Piljae Joo, Graduate Program of Energy Conversion and Storage, Ulsan National Institute of Science and Technology (UNIST),

Recently 2-dimensional (2D) materials such as graphene and transition metal dichalcogenides for electronics, green energy, and biomedical applications are widely researched owing to their outstanding physical and chemical properties. Herein, we study ‘top-down’ approached 2D materials and their multilayers by using layer-by-layer assembly for graphene based electrical devices and super-lattice structured transition metal dichalcogenides. The resulting multilayered materials are analyzed by various instruments such as scanning electron microscope, atomic force microscopy, UV/vis spectroscopy, raman spectroscopy, x-ray photoelectron spectroscopy.

Contents

Chapter 1.	Layer-by-Layer Assembled Graphene Field-Effect Transistor and Sensor Applications	
1.1	Abstract	7
1.2	Introduction	8
1.2.1	Low-Dimensional Carbon materials	8
1.2.2	Graphene in Electronic Properties	9
1.2.3	Graphene synthesis	9
1.2.4	Advantages of Layer-by-Layer Assembled Graphene	10
1.2.5	UV responsive molecule (spiropyran)	11
1.3	Experimental	15
1.3.1	Graphene oxide synthesis	15
1.3.2	Fabrications of graphene oxide by using Layer-by-Layer assembly	15
1.3.3	Spiropyran-pyrene synthesis	16
1.3.4	Electrode depositions	16
1.4	Results and Discussion	18
1.4.1	Surface analysis in affordance with different reduction methods	18
1.4.2	Characteristics of electronic Properties	20
1.5	Summary	30
1.6	References	31
Chapter 2.	Possibilities of 2D Layered Transition Metal Dichalcogenide Multilayers by Using Layer-by-Layer Assembly	
2.1	Abstract	36
2.2	Introduction	37
2.2.1	Solution process of layered transition metal dichalcogenides	37
2.3	Experimental	42
2.3.1	Preparation of metal dichalcogenide solutions	42
2.3.2	Fabrications of metal dichalcogenide multilayers	42
2.4	Results and Discussion	43
2.5	Summary	49
2.6	References	50
Acknowledgement		53

List of Figures

Figure 1-1 Various carbon-based nanomaterials produced with a graphene sheet as a basic building block.¹ (Geim and Novoselov, *Nat. Mater.* **2007**, *6*, 183)

Figure 1-2 Synthesis, etching and transfer process for the large scale and patterned CVD growth graphene films.² (Kim et al., *Nature* **2009**, *457*, 706)

Figure 1-3 Chemically exfoliated graphene from graphite.³ (1) Oxidation of graphites to graphite oxide with an increased interlayer distance. (2) Exfoliation of graphite oxides in water by sonication to obtain negatively charged GO colloids that are stabilized by electrostatic repulsion. (3) Controlled conversion of GO colloids to electrically conducting reduced graphene oxide colloids through removal of oxygen species with hydrazine. (Li et al., *Nat. Nanotechnol.*, **2008**, *3*, 101)

Figure 1-4 (a) Schematic illustration of the layer-by-layer (LbL) assembled multilayer film deposition process based on electrostatic interaction. (b) A simplified multilayer film built up from a negatively charged substrate.⁴ (Hong et al., *Nanoscale*, **2011**, *3*, 4515)

Figure 1-5 The switching cycle associated with the three states spiropyran (SP), merocyanine (ME), and protonated merocyanine (MEH).⁵ (Raymo and Giordani, *J. Am. Chem. Soc.* **2001**, *123*, 4651)

Figure 1-6 UV/vis absorbance spectra of (a) GO, (b) TRGO, and (c) CRGO films with different numbers of graphene bilayers on quartz substrates.

Figure 1-7 Ellipsometry measurements of GO, TRGO, and CRGO films with different numbers of graphene bilayers on SiO₂ substrates.

Figure 1-8 AFM images of (a) GO, (b) CRGO, and (c) TRGO films with various numbers of bilayers. The number in each figure represents the average root-mean-square surface roughness (R_{rms}).

Figure 1-9 (a) High-resolution XPS C1s and N1s spectra of 2-bilayer TRGO, CRGO, and GO films. Arrows indicate C_{sp2}-N in C1s and graphitic-N, pyrrolic-N, and pyridinic-N in N1s, respectively, after thermal reduction. (b) High-resolution XPS C1s and N1s spectra of TRGO films with various numbers of graphene bilayers. (c) Atomic ratio of C_{sp2}-N C and graphitic-N obtained from XPS C1s and N1s spectra of TRGO films.

Figure 1-10 Raman spectra of CRGO and TRGO films with various numbers of graphene bilayers.

Figure 1-11 Transfer characteristics of (a) TRGO, (b) CRGO FETs with various numbers of graphene bilayers (c) Minimum conductance of TRGO FETs as a function of number of graphene bilayers. (d) Dirac voltage changes in TRGO and CRGO based FETs as a function of number of graphene bilayers.

Figure 1-12 Transfer characteristics of the SP functionalized 2-bilayer graphene FETs ($V_D = -0.1$ V) upon (a, b) UV and (c, d) white light irradiation. (b, d) The right panels show the corresponding changes of the carrier mobilities and Dirac voltage as a function of the UV and white light irradiation time.

Figure 1-13 (a-c) Transfer characteristics of the SP-functionalized 2, 4, and 6-bilayer graphene FETs ($V_D = -0.1$ V) (black) before and (blue) after UV irradiation for 5 min. (d) Dirac voltage shift ($-\Delta V_{\text{Dirac}}$) and minimum conductance ratio ($G_{\text{UV}}/G_{\text{white}}$) between UV and white light irradiation as a function of the number of bilayers. The lines in (a-c) are included to aid the Dirac voltage shift and conductance changes. All values were reported with three independent measurements.

Figure 1-14 Time-course measurements of drain current of (a) SP-functionalized and (b) unmodified 2-bilayer graphene multilayer FET ($V_D = -0.1$ V and $V_G = -5$ V). Alternating irradiation cycles with UV and visible white light were employed during the measurements.

Figure 2-1 illustrations of $\text{MoO}_3\text{-MoS}_2$ hydrogen evolution catalyst.⁶ (Chen et al., *Nano Lett.* **2011**, *11*, 4168)

Figure 2-2 illustrations of phototransistor using MoS_2 thin films.⁷ (Lee et al., *Nano Lett.* **2012**, *12*, 3695)

Figure 2-3 TEM images of exfoliated nanosheets to the solvent assist method.⁸ (A to C) Low resolution TEM images of flakes of BN, MoS_2 , and WS_2 , respectively. (D to F) High-resolution TEM images of BN, MoS_2 , and WS_2 monolayers (Insets) Fast Fourier transforms of the images. (G to I) Butterworth-filtered images of sections of the images in (D) to (F) (Coleman et al., *Science* **2011**, *331*, 568)

Figure 2-4 Films of exfoliated MoS_2 nanosheets *via* lithium intercalation.⁹ (a) Photograph of MoS_2

film floating on water (top panel) and deposited on glass (bottom panel) (b) Photograph of an asdeposited thin film of MoS₂ on flexible PET. The films in (a) and (b) are approximately 5 nm thick (c) AFM image of an ultrathin film with an average thickness of 1.3 nm. The film consists of regions that are covered by monolayers and others that are slightly thicker due to overlap between individual sheets. Height profile along the red line is overlaid on the image. (Eda et al., *Nano Lett.* **2011**, *11*, 5111)

Figure 2-5 Low (a) and high (b) magnified SEM images of MoS₂ multilayer films with various numbers of bilayers.

Figure 2-6 XPS analysis of the 1 BL MoS₂ film on SiO₂/Si wafer (a) survey scan (b) Mo (C) S.

Figure 2-7 (a - d) Raman spectra of annealed MoS₂ thin films (e) height of intensity, (f) integrated intensity, and (g) peak frequency with different number of bilayers.

Figure 2-8 UV/vis absorbance spectra of following different numbers of MoS₂ bilayers on quartz substrates (a) Low and (b) high magnified.

Figure 2-9. Normalized PL spectra and integrated PL intensity differences of MoS₂ multilayer films with different numbers of bilayers.

List of Schemes

Scheme 1-1 Schematic representation of LbL assembled graphene based FETs.

Scheme 1-2 (Left) Schematic representation of the photoresponsive spiropyran functionalized layer-by-layer (LbL) assembled graphene multilayer FET structures (Right) chemical structures of positively and negatively charged graphene oxide nanosheets (GO^+ and GO^-) and pyrene-functionalized spiropyran (SP).

Scheme 2-1 Schematic representation of layer-by-layer assembled MoS_2 multilayer.

Chapter 1. Layer-by-Layer Assembled Graphene Field-Effect Transistor and Sensor Applications

1.1 Abstract

We demonstrate an easily controllable method to tune the charge transport in graphene field-effect transistors based on alternatively deposited positively charged and negatively charged graphene oxide using layer-by-layer assembly. Interestingly, tuning the number of bilayers of thermally reduced graphene oxide multilayer films allowed achieving either ambipolar or unipolar (both *n*- and *p*-type) transport in graphene transistors. Based on X-ray photoemission spectroscopy, UV-vis spectroscopy, Raman spectroscopy, and electronic measurements, we found that nitrogen atoms from the functional groups of positively charged graphene oxide are incorporated into the reduced graphene oxide films and substitute carbon atoms during the thermal reduction in different degrees for graphene multilayers. In addition, we introduce pyrene modified spiropyran and layer-by-layer assembled graphene multilayer composite based the sensor. Moreover, spiropyran decorated graphene multilayers performed as the degree of doping tuned UV sensors.

1.2 Introduction

In recent years, a two-dimensional carbon lattice structured material, graphene, has been widely researched. Its superior mechanical, chemical, thermal, and electrical properties are attractive into various fields.^{1,2,10-13} Particularly, superior electrical properties showing high theoretical carrier mobility and conductivity make graphene the first candidate for flexible electronics and sensors.¹⁴⁻¹⁹

Since Novoselov and Geim focused on incorporating graphene into a field-effect transistor (FET), many efforts have developed by complicated logic gates based on graphene FETs towards achieving high speed integrated electronic circuits.²⁰⁻²² In a practical point of view, solution-based methods have been developed to deposit graphene onto various substrates which provides versatile opportunities to employ graphene in low-cost, flexible electronic applications.

Moreover, achieving unipolar transport in graphene (*n*- and *p*-type transport separately) is critical, because employing both *n*- and *p*-type unipolar transport devices in a complementary manner is highly desirable for complex logic circuits compared to those based on ambipolar transport. According to various recent efforts to access unipolar conduction in graphene, including tuning the bandgap *via* width-controlling nanoribbons,²³⁻²⁶ introducing impurities or chemical doping,²⁷ controlling the interface polarization *via* self-assembled monolayer,^{28,29} and controlling the charge-density pinning effect at metal contacts.^{30,31} Although a moderate shift in the Dirac voltage and a slight enhancement/suppression in the respective carrier mobility were observed, many of these approaches still yielded an ambipolar transport behavior in graphene. Recently, it is reported a complementary logic inverter based on true *n*- and *p*-type unipolar graphene transistors by controlling the doping density in graphene using titanium oxide by Li and co-workers.³²

In addition, non-covalent functionalization of graphene has been known to be a versatile protocol in introducing other functional molecules and biomolecules on the surface of graphene, while still preserving the innate structure of graphene.³³⁻³⁵

1.2.1 Low-dimensional carbon materials

In the last few decades, research about low-dimensional carbon based materials such as fullerene (0D), carbon nanotube (1D), and graphene (2D) has been dramatically advanced because of abundance in nature, possible modification by physical and chemical treatments, and their novel properties (**Figure 1-1**).^{1,36,37}

A fullerene consists of sp^2 hybridized carbon atoms, in the form of a spherical hollow structure also called a buckyball. The first discovery of fullerene was in 1985 by Richard Smalley and co-workers, and they named the new material to buckminsterfullerene (C_{60}).^{36,38}

Carbon nanotubes (CNTs) which discovered by Iijima in 1991 are cylindrical structured carbon materials.³⁹ Because of their outstanding mechanical, thermal, and electrical properties, these cylindrical carbon molecules superior properties for nanotechnology, electronics related science fields.³⁷ CNT's are rolled from sp^2 -hybridized hexagonal carbon sheets at specific angles, and the combination of the rolling angle and radius consequently determines the specific properties; for instance, single sheets of rolled nanotubes can indicate conducting or semiconducting behavior.³⁷ Also, CNTs are categorized to the different number of shells as single-walled nanotubes (SWNTs) and multi-walled nanotubes (MWNTs).³⁷ Although CNTs have amazing properties in thermal, mechanical, and electronic properties, separation to individual nanotubes are obstacles due to van der Waals forces, more specifically, π -stacking themselves for researches and applications.^{40,41}

Graphene is a regularly arranged planar sheet of sp^2 -hybridized hexagonal carbon lattice structured material as a single sheet of graphite. It is also an allotrope of low-dimensional carbon and has superior thermal, mechanical, electrical properties as CNTs.^{1,2,10-13} Since Geim and Novoselov successfully exfoliated a single layer graphene from graphite flakes in 2004, graphene has become an extremely highlighted material owing to its novel applications such as nanotechnology, electronics, and other fields.^{1,22}

1.2.2 Graphene in electronic properties

Developments of electronic devices, especially of silicon-based transistors, lead to improve our life quality, and we demand smaller, faster, and more versatile electronics with saving energy.⁴² However, practically, silicon-based devices may not fully gratify our needs due to its fundamental and technical limitations of power-consumption, denser package, and faster speed.⁴²

Carbon based material become one of the rising-star to substitute silicon based devices to overcome the limitations of conventional devices. Representatively, low-dimensional carbon materials like CNTs and graphene are strongly recommended for the future electronics with their electronic performance.⁴²

Theoretically, graphene reveals tunable charge carrier with ambipolar electric field effect between electrons and holes. The concentration of charge n is upon 10^{13} cm^{-2} and their mobilities μ can be over $15,000 \text{ cm}^2 \text{ V}^{-1} \text{ s}^{-1}$ under ambient conditions. In addition, depending on temperature T , the carrier mobilities can be possibly improved up to $\approx 100,000 \text{ cm}^2 \text{ V}^{-1} \text{ s}^{-1}$.¹

1.2.3 Graphene synthesis

Since Novoselov and Geim experimentally studied graphene which exfoliated graphite flakes to

'Scotch tape' method,²² other obtaining graphene methods have been proposed: chemical vapor deposition (CVD) growth,^{2,43} epitaxial growth,^{44,45} solvent-assist,⁴⁶ and oxidation method for mass productions.^{3,12,47}

A chemical vapor deposition method with Cu or Ni catalyst is well known graphene synthesis method.^{2,43} A synthesis of graphitic carbon thin films has been researched for over 40 years with hydrocarbon sources on catalysts. Since large scale CVD growth graphene was introduced in 1999 by Hong and co-workers, it has been tremendously researched to replace indium tin oxide (ITO) for electronic applications (**Figure 1-2**).²

Epitaxial growth graphene on silicon carbide is also well optimized method.^{44,45} However, quality of epitaxial growth graphene is not enough for electronics to compare with CVD growth and mechanically exfoliated graphene.² Moreover, silicon carbide substrate and growth condition up to 1500 °C are high cost for mass production in industry.

Solution processes such as solvent-assisted method and oxidation method to isolate graphene have great advantages for large scale and easy process in industry. However, the solvent-assisted exfoliation of graphene might exfoliate single layers.⁴⁶ Therefore, practically, the oxidation of graphite with ultrasonication is popularly used to collect large scale graphene sheets.^{3,12,47} Representative oxidation methods are Brodie,⁴⁸ Staudenmaier,⁴⁹ and Hummers method using strong acids and oxidants.⁵⁰ After ultrasonication of oxidized graphite in water, lots of isolated graphene sheets with diverse functional groups such as ketone, hydroxyl, epoxy, and carboxylic acid appear.⁵¹ Although well dispersed large amount graphene sheet owing to functional groups in water can be collected from oxidation method, an army of defect interrupts charge transport when GO is used to electronics. Chemical reduction to remove epoxy or thermal reduction to eliminate every functional group is inevitable to restore electronic properties of GO (**Figure 1-3**).^{3,47,52} Even though many efforts to make perfectly restored structure from GO, reduced graphene oxide (rGO) could be not reached high enough performance in electronic application due to originally collapsed structures. Despite low electrical properties, rGO has huge potential to use catalysts and electronics in industry with its easy process, high yield, and outstanding affinity with other materials.

1.2.4 Layer-by-Layer assembly of carbon materials

Since earlier Iler⁵³ and later Decher introduced LbL assembly,⁵⁴ it has been studied as the most versatile method to assemble multifunctional nanoscale materials such as metal, inorganic, and organic materials (**Figure 1-4**).^{4,55} The basic LbL assembly method is that counter charged materials on the surface are alternatively deposited on charge imposed substrates with several times washing process. This process can easily make the order and thickness controlled composite films.⁵⁴

After huge potentials of carbon materials are notified in nanoscale science, controlling the distinct structure and composition become hot issue. Due to simplicity and versatility of the LbL assembly has rapidly emerged as a high functional surface coating technique. Because of their special physical, chemical, and mechanical properties, carbon nanomaterials such as fullerenes (0D), carbon nanotubes (1D), and graphenes (2D) present chance to design versatile thin surface for catalysts, biosensors, electronic applications.⁴ Even though other methods are possibly used to fabricate carbon materials such as vacuum filtration and chemical vapor deposition, the LbL assembly is popularly researched because of the simplicity and robustness.⁴

1.2.5 UV responsive molecule (spiropyran)

Photo-responsive molecules have long been designed the natural photoconduction processes.⁵⁶⁻⁵⁸ Among the diverse photo-responsive molecules such as diaryletene, stilbene, and spiropyran, spiropyran is a well-known photochromic molecule with its interesting tunability, stability and fast response (**Figure 1-5**).⁵ For example, colorless spiropyran undergoes reversible transformation to purple-colored merocyanine upon UV irradiation with dipole moment changes and the structural conversions from neutral to charge separated zwitterion. Because of its interesting photoresponsive properties, spiropyran has been employed in optical sensors and memory devices.⁵⁹ Kim and co-workers reported the reversible modulation of transport behavior of SWNT based FETs that are modified with spiropyran-based molecular switches.⁶⁰

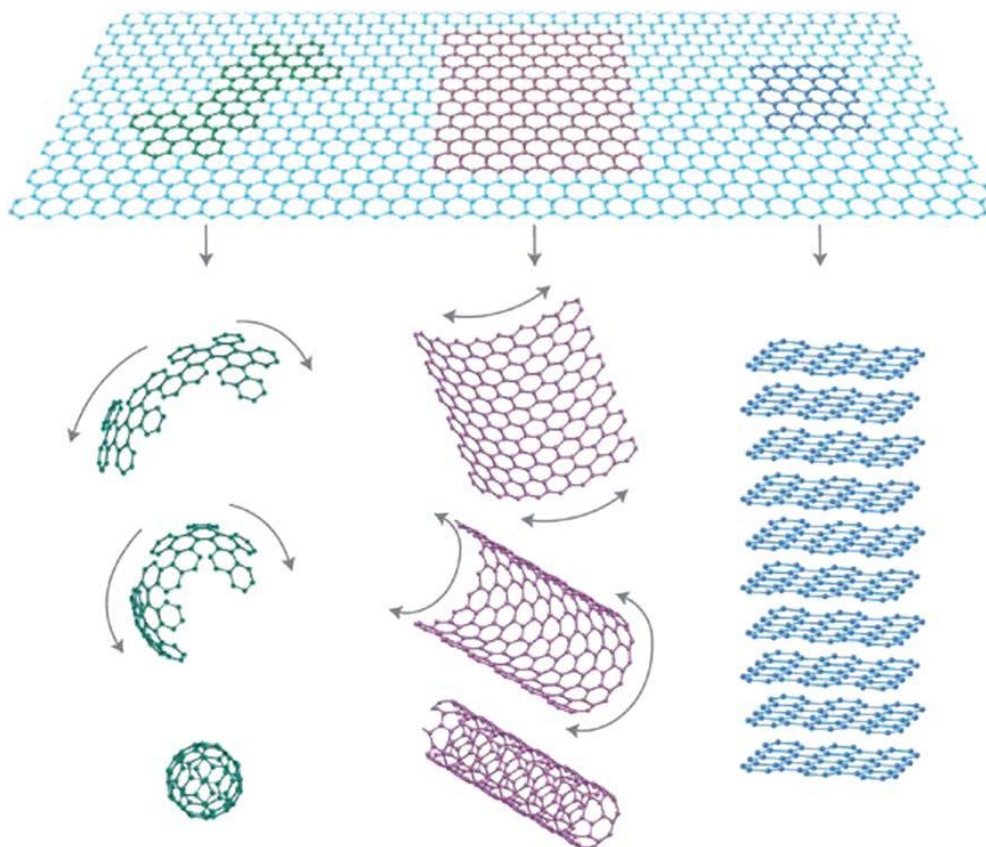


Figure 1-1 Various carbon-based nanomaterials produced with a graphene sheet as a basic building block.¹ (Geim and Novoselov, *Nat. Mater.* **2007**, *6*, 183)

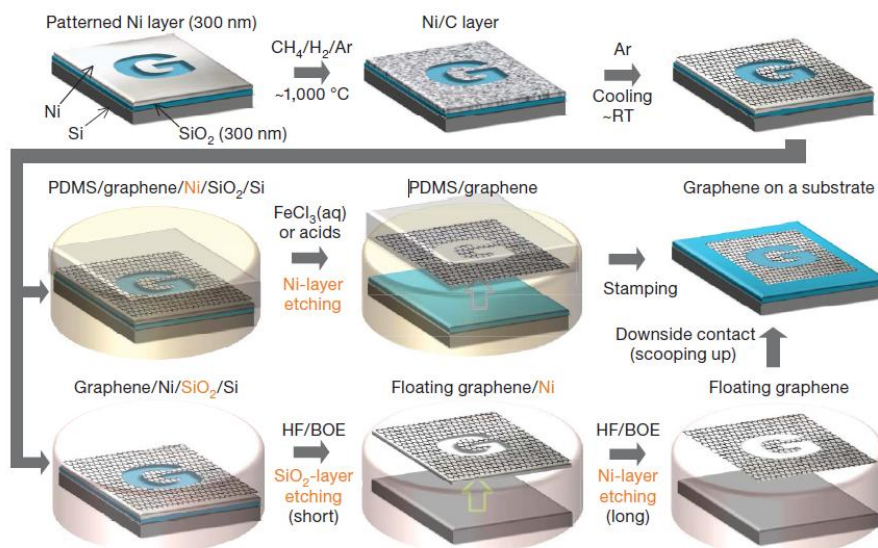


Figure 1-2 Synthesis, etching and transfer process for the large scale and patterned CVD growth graphene films.² (Kim et al., *Nature* **2009**, *457*, 706)

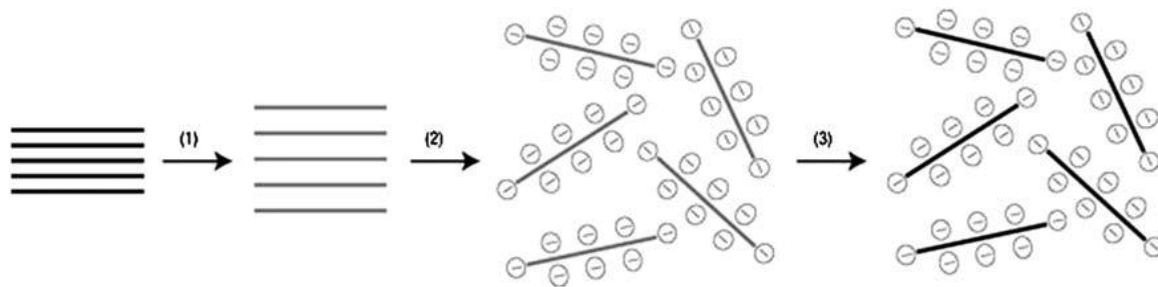


Figure 1-3. Chemically exfoliated graphene from graphite.³ (1) Oxidation of graphites to graphite oxide with an increased interlayer distance. (2) Exfoliation of graphite oxides in water by sonication to obtain negatively charged GO colloids that are stabilized by electrostatic repulsion. (3) Controlled conversion of GO colloids to electrically conducting reduced graphene oxide colloids through removal of oxygen species with hydrazine. (Li et al., *Nat. Nanotechnol.*, **2008**, 3, 101)

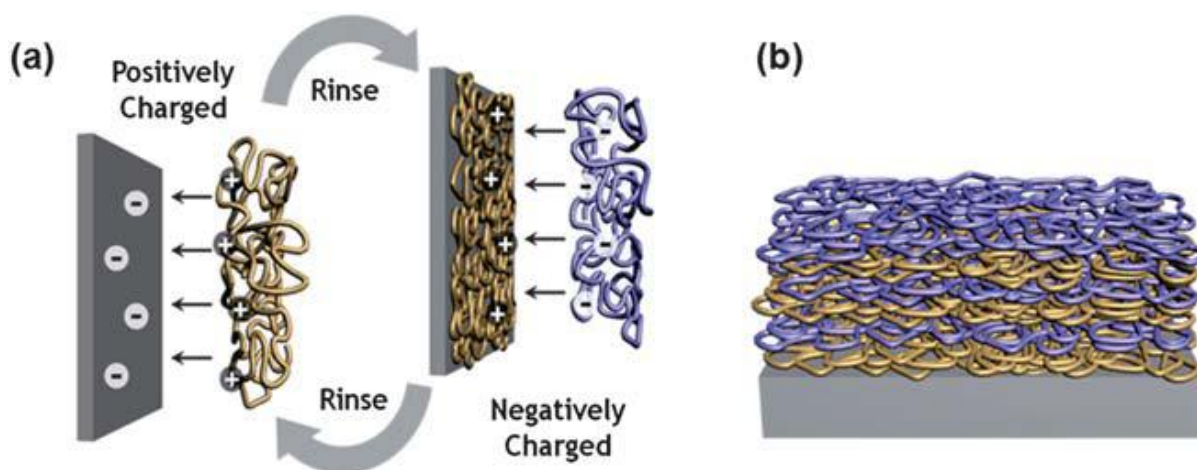


Figure 1-4 (a) Schematic illustration of the layer-by-layer (LbL) assembled multilayer film deposition process based on electrostatic interaction. (b) A simplified multilayer film built up from a negatively charged substrate.⁴ (Hong et al., *Nanoscale*, **2011**, 3, 4515)

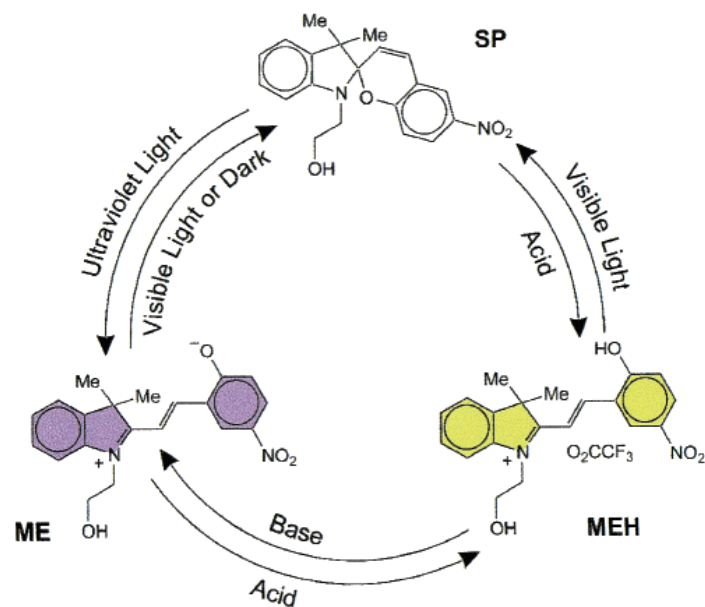


Figure 1-5 The switching cycle associated with the three states spiropyran (SP), merocyanine (ME), and protonated merocyanine (MEH).⁵ (Raymo and Giordani, *J. Am. Chem. Soc.* **2001**, 123, 4651)

1.3 Experimental

1.3.1 Graphene oxide synthesis

Graphite oxide was synthesized from graphite powder (Bay Carbon Sp-1 grade) by the modified Hummers method^{50,61} and exfoliated to give a brown dispersion of GO under ultrasonication. Briefly, graphite powders (1.0 g), $K_2S_2O_8$ (0.50 g) and P_2O_5 (0.50 g), were added to 3.0 mL of conc. H_2SO_4 with stirring until the reactants are completely dissolved. The mixture is kept at 80 °C for 4.5 h, after which the heating is stopped and the mixture diluted with 1.0 L of Millipore water. The mixture is filtered and washed to remove all traces of acid. For the oxidation step of the synthesis, the pretreated graphite is added to the 26mL of H_2SO_4 and stirred. To this reaction mixture, 3.0 g of $KMnO_4$ was added slowly in an ice bath to ensure that the temperature remained below 10 °C. Then, this mixture reacts at 35 °C for 2 h after which 46mL of distilled water is added under an ice bath. This mixture is stirred for 2 h at 35 °C, after which the heating is stopped and the mixture diluted with 140mL of water and 2.5 mL of 30% H_2O_2 is added to the mixture resulting in a yellow color along with bubbling. The mixture is allowed to settle for at least a day after which the clear supernatant is decanted. The remaining mixture is filtered and washed with a 1.0 L of 10% HCl solution. The resulting solid is dried in air and diluted in distilled water that is put through dialysis for 2 weeks to remove any remaining materials and residues, after which the product was centrifuged and washed several times with Millipore water to neutralization and remove residual species. Finally, the dark brown GO powders were obtained through drying at 50 °C in a vacuum oven for a day. The GO powder dissolved in a known volume of water is subjected to ultrasonication for 30 min to give a stable suspension of GO (typically conc. 0.50 mg/mL) and then centrifuged at 4000 rpm for 10 min to remove any aggregates remained in the suspension.

1.3.2 Fabrications of graphene oxide by using Layer-by-Layer assembly

The multilayer graphene films were prepared by sequential LbL assembly between positively and negatively charged GO sheets and subsequent thermal (or chemical) reduction. Negatively charged graphene oxide suspensions (GO^-) were prepared according to the modified Hummers method with pure graphite followed by exfoliation under ultrasonication. Separately, positively charged stable GO suspensions (GO^+) were prepared by introducing amine groups (NH_2) on the surface of negatively charged GO sheets through the *N*-ethyl-*N'*-(3-dimethyl aminopropyl)carbodiimide methiodide (EDC)-mediated reaction between carboxylic acids (and/or epoxides) and excess ethylenediamine ($NH_2CH_2CH_2NH_2$). As-prepared respective GO suspensions exhibited a fairly good colloidal stability

over a wide span of pH conditions. They also displayed the changes of zeta-potential in response with external pH conditions which is a typical pH-responsive feature for weak polyelectrolytes. With these two stable suspensions of GO^+ and GO^- , we have fabricated GO multilayer films by repeatedly spin-coating onto a planar SiO_2/Si substrate or a quartz slide to afford the multilayer in an architecture of $(\text{GO}^+/\text{GO}^-)_n$ (n = number of bilayers, typically $n = 2 - 6$) (**Scheme 1-1**). Finally, the GO multilayers were subjected to either thermal reduction process (1000 °C) under Ar or chemical hydrazine reduction to afford multilayers of RGO following well-documented protocol.

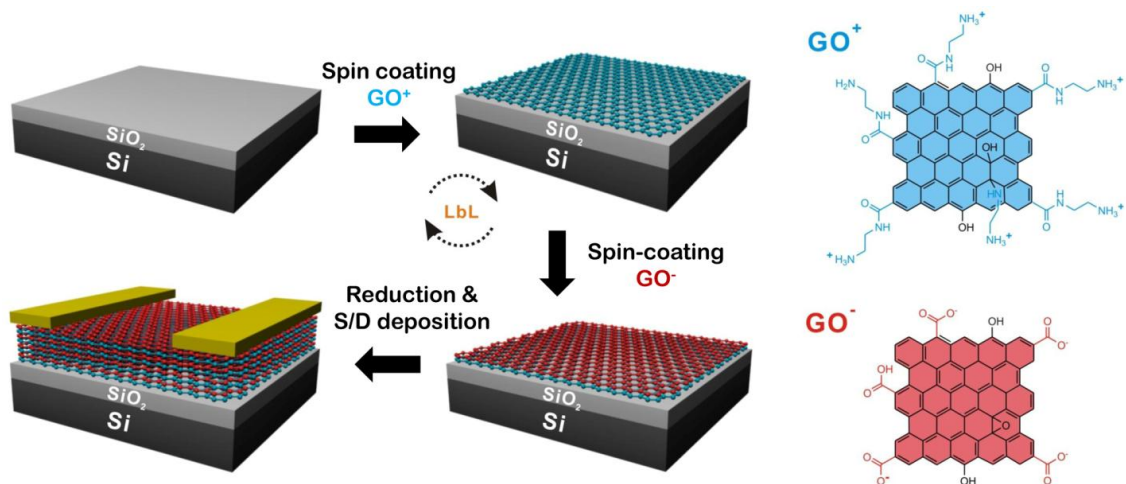
1.3.3 Spiropyran-pyrene synthesis

For the functionalization of graphene multilayer films, non-covalent π - π interaction based on pyrene moiety was employed as it has been traditionally used for the functionalization of graphitic layers. Spiropyran was initially prepared by following a literature.⁵ Spiropyran (0.253 g, 0.72 mmol) was dissolved in dichloromethane (15.0 mL) after which N,N' -dicyclohexylcarbodiimide (0.221 g, 1.1 mmol), 4-dimethyl aminopyridine (8.74 mg, 0.07 mmol) and 1-pyrenebutyric acid (0.309 g, 1.1 mmol) were added over an ice bath. And then, the solution was stirred for 24 h at room temperature. The resulting white precipitate was filtered off and the filtrate was extracted with dichloromethane. The combined product mixture washed with aqueous NaHCO_3 and water and dried over MgSO_4 . The organic phase was concentrated under reduced pressure, and the crude product was purified by silica gel column chromatography (Hexane/EtOAc = 5/1, $R_f = 0.5$). The product was obtained as a yellow solid (0.24 g, 53.6%). ^1H NMR (600 MHz, CDCl_3): δ (ppm) = 7.78-8.28 (11H, m, ArH), 6.62-7.20 (6H, m, ArH), 5.76 (1H, d, $J=10.2$ Hz, ArH), 4.14-4.29 (2H, m), 3.30-3.49 (4H, m), 2.32-2.43 (2H, m), 2.10-2.19 (2H, m), 1.23 (3H, s), 1.09 (3H, s)

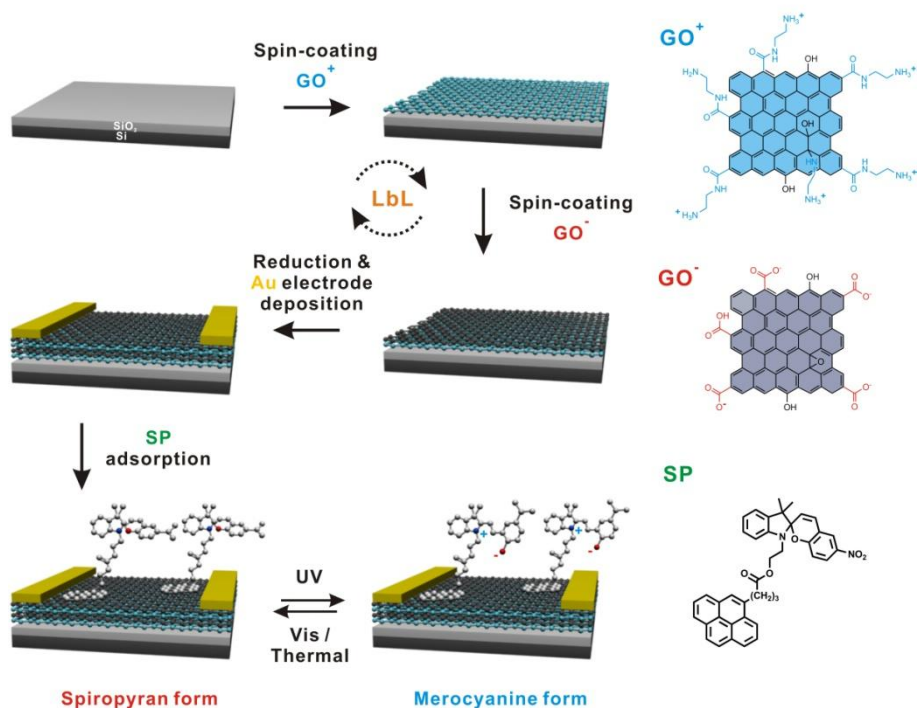
The synthesized SP molecules in ethyl acetate were deposited with gentle washing on chemically and thermally (300 °C) reduced 2-6 BL GO films for UV sensor applications (**Scheme 1-2**).

1.3.4 Electrode depositions

The electrical characteristics of the as-prepared LbL assembled graphene films were investigated by employing graphene FETs. Specifically, the graphene FETs were fabricated by assembling multilayer graphene films on a heavily doped Si wafer with a thermally grown 300 nm-thick SiO_2 layer. The Si wafers itself and the SiO_2 layer worked as the gate electrode and the gate dielectric, respectively. Au contacts that were deposited on top of the graphene film by thermal evaporation served as the source and drain electrodes. The channel length (L) and channel width (W) were 100 and 800 μm , respectively.



Scheme 1-1 Schematic representation of LbL assembled graphene based FETs.



Scheme 1-2 (Left) Schematic representation of the photoresponsive spiropyran functionalized layer-by-layer (LbL) assembled graphene multilayer FET structures (Right) chemical structures of positively and negatively charged graphene oxide nanosheets (GO^+ and GO^-) and pyrene-functionalized spiropyran (SP).

1.4 Results and Discussion

1.4.1 Surface analysis in affordance with different reduction methods

The successful growth of GO multilayers was displayed from a gradual increase of the UV/vis absorbance spectra with a characteristic absorbance of GO within the multilayer films at 222 nm (**Figure 1-6a**). This peak shifts to 275 and 268 nm after thermal and chemical reduction, respectively, which indicates the successful restoration of electronic conjugation within the graphene sheets (**Figure 1-6b and c**).³ The UV/vis absorbance spectra of the corresponding TRGO and CRGO films also exhibited a gradual increase with increasing number of BL.

Also, the ellipsometry measurement showed that the thickness of GO multilayer films is linearly proportional to the number of bilayers, demonstrating true LbL assembly of GO multilayers (**Figure 1-7**). Note that the thickness of GO films decreased upon chemical or thermal reduction due to the loss of surface functional groups.⁶² From the linear fitting of the curves, the average BL thickness of GO, TRGO, and CRGO is calculated to be 1.6, 0.6, and 1.1 nm, respectively.

The atomic force microscopy (AFM) images of 2-6 BL GO (**Figure 1-8a**), CRGO (**Figure 1-8b**), and TRGO (**Figure 1-8c**) films show surface morphologies. Initial few layer depositions (less than 2 BL) displayed overlaid sheets of GO, though the complete substrate was not covered as often observed in initial few layers of polyelectrolyte-based LbL systems. As the deposition progresses more than 3-bilayers, however, the entire surface was uniformly covered with GO. Interestingly, the edges of individual graphene sheets are clearly visible in an as-assembled GO multilayer film, whereas the individual sheets appear to merge together and leave no distinct boundary between each sheet after thermal annealing. In addition, surface root-mean-square roughness (R_{rms}) values (averaged over $10 \times 10 \text{ m}^2$) of 2 and 6 BL were determined to be 1.4 and 2.5 nm, respectively. After thermal reduction, these values decreased to 0.4 and 0.8 nm, respectively. The decreased surface roughness is ascribed to the reorientation of GO sheets and densification of the thin film during thermal annealing.

To study the influence of thermal annealing and the origin of consequent electron doping, we have employed several independent techniques. First, X-ray photoemission spectroscopy (XPS) was performed to investigate the changes of chemical functional groups during the thermal (and chemical) reduction process. **Figure 1-9a** shows the high-resolution XPS spectra of the 2-bilayer TRGO, CRGO, and GO films. The deconvoluted C1s spectra of GO film exhibited five distinct components, including sp^2 -hybridized carbons (284.5 eV), C–O in epoxy and hydroxyl (286.2 eV), carbonyls (286.8 eV), amides (287.9 eV), and carboxylic acids (288.9 eV), which are all in good agreement with previous reports.⁶³⁻⁶⁵ The intensities of the peaks assigned to the oxygen-bearing functional groups such as hydroxyl, epoxy and carbonyl groups almost disappeared after thermal reduction, as expected.

Interestingly, a new peak located at 285.9 eV appeared, corresponding to C–N with sp^2 -hybridized carbon,⁶⁴ albeit the thermal reduction was performed in a nitrogen-free condition. In contrast, after chemical reduction, the peak associated with the C–N with sp^2 -hybridized carbon was not observed, although peaks from oxygen moieties were removed considerably. These results indicate that the nitrogen atoms in amide and amine groups within the positively charged GO are incorporated into the graphene layer and substitute carbon atoms only during the thermal annealing process. Furthermore, we found that the relative amount of carbon atoms yielding C_{sp^2} -N (285.9 eV) signal increases with increasing number of BL (**Figure 1-9b** and **c**). This result suggests that more nitrogen atoms are introduced into the graphene as the film thickness increases.

In accord with the above results, N1s spectra yielded more detailed information about the change in the chemical states of graphene films after thermal (and chemical) reduction. The N1s peak in the 2-bilayer GO film has two components centered at 399.6 and 402.5 eV, corresponding to amides and amines, respectively, which arise from the chemically modified positively charged GO (**Figure 1-9a**). Interestingly, new types of nitrogen species appeared after thermal reduction at 398.6, 400.3, and 401.1 eV, which can be assigned to pyridinic-N, pyrrolic-N, and graphitic-N, respectively.^{64,65} In contrast, these new peaks were not observed after chemical reduction with hydrazine, although the signal corresponding to amines were dramatically reduced. These new peaks supports that the N atoms are doped into the graphene lattice after thermal reduction at high temperature. Also, the relative amount of graphitic-N (401.1 eV) increased with number of bilayers in TRGO films, reflecting more substitutional nitrogen doping into graphitic layer for thicker films (**Figure 1-9b and c**). From the XPS measurement, we estimated approximately 1.64% nitrogen is doped into the 6-bilayer TRGO film. The explanation for such trend, which was also observed from the C1s XPS data and the electrical transport measurements, is as following. Nitrogen species such as amines and amides would be removed from the surfaces of graphene sheets, probably in the form of N_2 gas during the thermal annealing process as observed in other report.⁶⁶ However, the stacked and confined geometry of the LbL assembled multilayer films possibly prevents facile escape of the nitrogen species. Therefore, more fractions of nitrogen species are likely to reside within the film with more number of graphene layers and, thereby, resulting in a higher nitrogen-doping concentration per unit volume of carbon lattice. Although the detailed mechanism of nitrogen doping onto the multilayer graphene film is still elusive, note that a similar approach was employed in the synthesis of nitrogen-doped graphenes by mixing chemically modified graphene oxide with nitrogen-rich compounds like melamine under high temperature annealing process.⁶⁵ It should be noted that the number of bilayers is the key factor in modulating both the nitrogen doping level and electrical conductance of graphene films. These interesting features highlight the advantages of LbL assembly as a nanoscale bottom-up assembly technique that is otherwise hard to achieve with other methods.

Raman spectroscopy is the most direct and nondestructive technique to characterize the structure of carbon materials. CRGO films did not exhibit any shift in the G band upon varying the number of bilayers (**Figure 1-10a**). The evolution of the Raman spectra is presented in **Figure 1-10b** as a function of number of graphene bilayers in TRGO films. The Raman spectra were obtained with excitation at 532 nm for 10 s to avoid overheating of the samples. Significant red-shift (ca. 19 cm^{-1}) of the G band was observed as the number of graphene bilayers increased, while D band remained fixed. This red-shift of the G band implies electron doping effect in TRGO films, as it is suggested that electron doping up-shifts the Fermi level away from the Dirac point.⁶⁷⁻⁷⁰

1.4.2 Characteristics of electronic properties

Figure 1-11a shows the conductance (G) vs. V_G plots of TRGO FETs with different numbers of graphene bilayers. Surprisingly, we observed that the charge transport in TRGO FETs changes dramatically, along with an expected increase in the film conductance (**Figure 1-11b**), upon varying the number of bilayers. TRGO FETs with 2-bilayers exhibited unipolar p -type conduction, unlike typical graphene FETs that generally yield ambipolar transport.⁷¹ A similar result was observed previously from a mechanically cleaved monolayer graphene which was explained by a positive charge transfer from the SiO_2 substrate during thermal treatment.¹⁹ As the number of bilayers increased, the influence of the SiO_2 substrate was reduced concomitantly, while n -type conduction appeared gradually and the Dirac voltage shifted accordingly to more negative voltage (**Figure 1-11c**). As consequences, a symmetric ambipolar transport was observed from 5-bilayered TRGO films and even unipolar n -type conduction was observed from 6-bilayered TRGO films. These results indicated that more electron doping is taking place as the number of bilayers increases. Note that such a dramatic change in the charge transport from nearly p -type to ambipolar and even to n -type transport and a Dirac voltage shift of 133 V (from 78 V to -55 V) occurred only within difference of 4-bilayer of TRGO films. We also carried out a similar experiment based on LbL assembled CRGO FETs (**Figure 1-11b**). However, no significant change in the transport type or a shift in the Dirac voltage was observed upon varying film thickness (**Figure 1-11c**). These results suggest that n -type doping did not occur during the chemical reduction and that the thermal annealing during the reduction process plays an important role in electron doping of multilayer graphene films.

Additionally, we investigated UV responsive sensor to SP functionalized grapheme multilayer FETs. **Figure 1-12** shows the drain current (I_D) as a function of gate voltage (V_G), which is characteristic of SP functionalized 2 BL graphene multilayer FETs upon UV and white light illumination. The LbL-assembled graphene FETs without SP molecules showed a slight p -type behavior with a Dirac point of 3.6 V. Interestingly, however, the devices displayed a weak n -type

doping behavior with a Dirac point of -1.7 V upon the deposition of SP molecules. This is due to the net negative charge transfer from assembled SP to graphene multilayer, which is consistent with the previous result based on SP-functionalized SWNT.⁶⁰ This observation is, however, in clear contrast to typical p-type doping that are commonly induced by physical adsorbates such as oxygen and water during the preparation of graphene FETs.⁷² Upon UV irradiation, ring opening of spiropyran proceeds to zwitterionic merocyanine with a significant dipole moment increase (from ca. 4 to 20 D) that induces the development of localized dipole field on the surface of graphene FETs. This localized dipole field strongly influences the shift of the Dirac point. Moreover, the phenoxide ion created in the open merocyanine form can possibly enhance the development of negative charges near the graphene multilayers.⁷³ UV-induced n-doping of graphene FETs is further evidenced by the fact that the hole mobility is suppressed from 2.9 to 2.2 cm²/Vs while electron mobility remains almost constant at 2.6 cm²/Vs. (**Figure 1-12b and d**).⁷⁴

The Dirac voltage shift was also dependent on the irradiation time; for example, the initial Dirac voltage of -1.7 V became -4.7 V after 1 min and -10.2 V after 5 min. This shift is fully reversible upon irradiation with white light, which converts the merocyanine back to spiropyran with a subsequent recovery of the Dirac voltage. In contrast, the control experiment of unmodified graphene multilayer FETs did not show any sign of photoresponsive behaviour.

We then turn to the increase in minimum conductance upon UV irradiation. It is possible that the conjugation length of graphene multilayers containing many defect sites increased owing to ring opening of spiropyran to fully conjugated merocyanine, thus raising the density of charge carriers in the graphene channel.⁷³ In addition, the increased dipole moment of the merocyanine form leads to dielectric screening for an enhanced carrier mobility in graphene FETs as similarly observed by Tao and co-workers.⁷⁵

By taking advantages of the LbL assembly, we also observed that the degree of Dirac voltage shift (ΔV_{Dirac}) under UV illumination could be precisely tunable by the number of bilayers in graphene multilayers. As shown in **Figure 1-13**, interestingly, the shift in Dirac voltage was most pronounced in the 2-bilayer film, which then gradually decreased with an increased number of bilayers. For example, the Dirac voltage shifts of 11.3 and 4.1 V were observed from 2- and 5-bilayer graphene FETs upon UV radiation for 5 min, respectively. This result stems from the reduced influence of SP molecules to the interfacial graphene channel as the number of bilayers, which eventually becomes saturated after 6-bilayer of graphene multilayers. In accord with the Dirac voltage shift, the conductance change ratio of UV vs. white light illumination ($G_{\text{UV}}/G_{\text{white}}$) diminishes as the film continues to become thicker (**Figure 1-13d**). Taken together, this observation supports the argument that the observed photoresponsive effect is originated from the interaction between SP molecules and graphene surfaces. Moreover, it should be noted that the number of bilayers of graphene films is the

key factor in tuning both the degree of doping and electrical conductance of graphene films. These interesting features highlight the advantages of LbL assembly as a nanoscale bottom-up assembly that would have otherwise been hard to achieve with other techniques.

Finally, in order to investigate the kinetics of the photoswitching process of SP-functionalized graphene multilayer FETs, the I_D (at V_D of -0.1 V and V_G of 0 V) was monitored as a function of time (**Figure 1-14**). The illumination was switched between UV and visible light while measuring the device performance. The channel conductance increased gradually with UV irradiation but decreased with white light irradiation. Interestingly, the rate of conductance variation was found to be different for UV and white light exposure. Typically, after UV exposure for 5 min, a longer visible light irradiation time of 10 min was necessary to recover the original conductance. The ring opening of spiropyran by UV and recyclization by white light can be fitted with a single exponential function. The obtained decay time constant for ring opening was 135.9 ± 2.0 s, whereas that for recyclization was 327.8 ± 5.9 s. These values are comparable with those in the previous results based on the SWNT devices with spiropyran molecules.⁶⁰ In a clear contrast, control devices without SP modification did not exhibit any changes in conductance upon UV and visible light exposure, confirming the role of SP in the observed photoresponsive switching behavior **Figure 1-14b**.

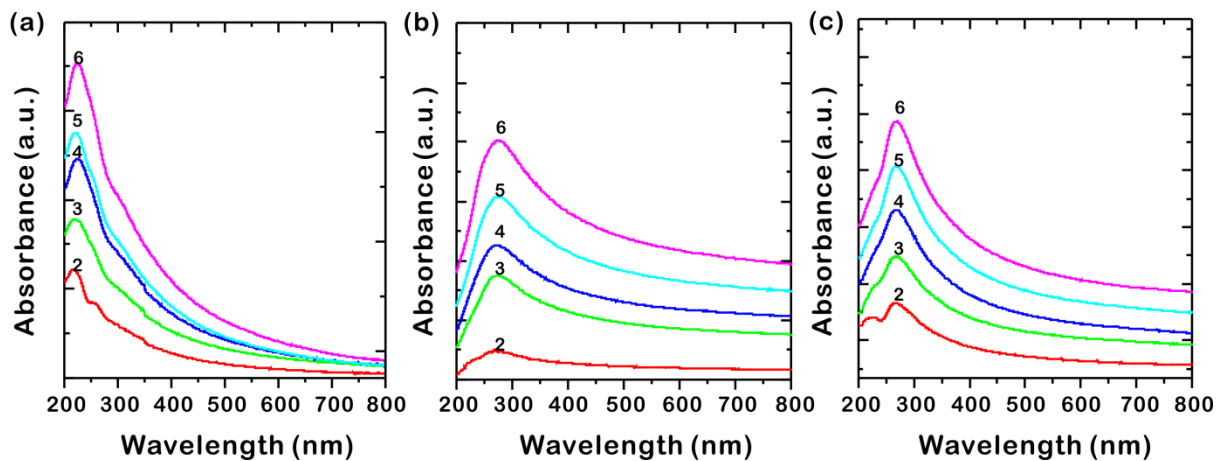


Figure 1-6 UV/vis absorbance spectra of (a) GO, (b) TRGO, and (c) CRGO films with different numbers of graphene bilayers on quartz substrates.

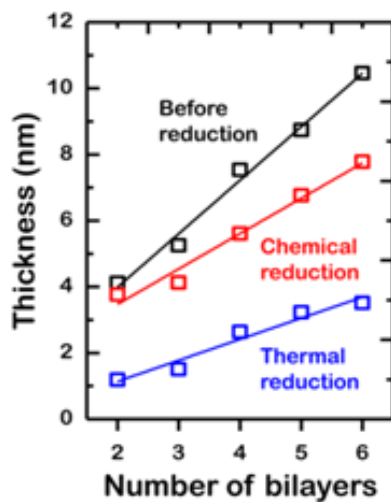


Figure 1-7 Ellipsometry measurements of GO, TRGO, and CRGO films with different numbers of graphene bilayers on SiO₂ substrates.

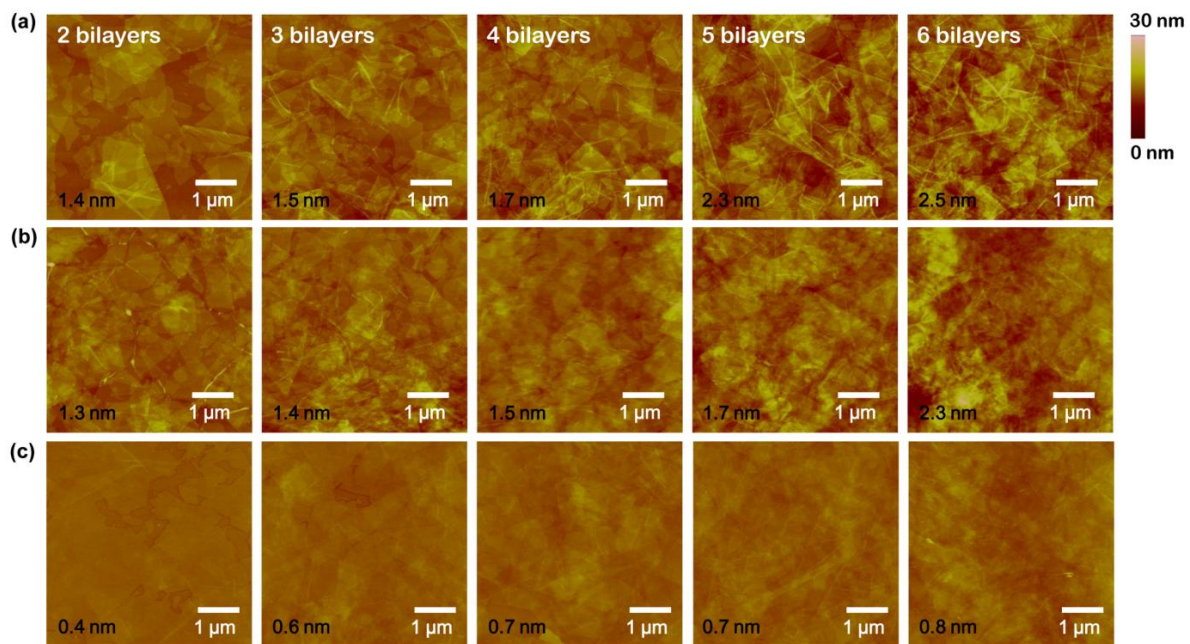


Figure 1-8 AFM images of (a) GO, (b) CRGO, and (c) TRGO films with various numbers of bilayers. The number in each figure represents the average root-mean-square surface roughness (R_{rms}).

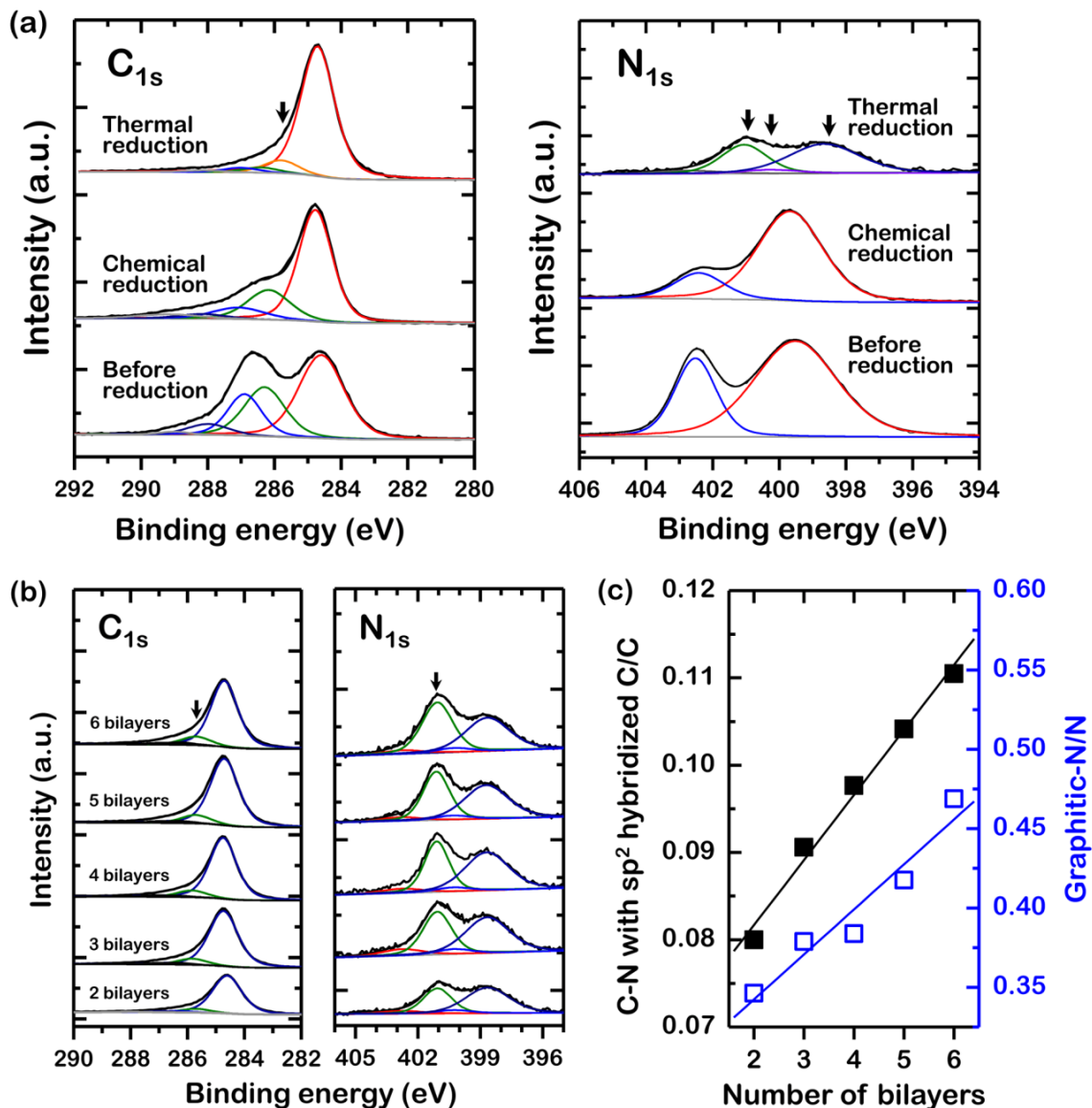


Figure 1-9 (a) High-resolution XPS C_{1s} and N_{1s} spectra of 2-bilayer TRGO, CRGO, and GO films. Arrows indicate C_{sp²-N} in C_{1s} and graphitic-N, pyrrolic-N, and pyridinic-N in N_{1s}, respectively, after thermal reduction. (b) High-resolution XPS C_{1s} and N_{1s} spectra of TRGO films with various numbers of graphene bilayers. (c) Atomic ratio of C_{sp²-N} C and graphitic-N obtained from XPS C_{1s} and N_{1s} spectra of TRGO films.

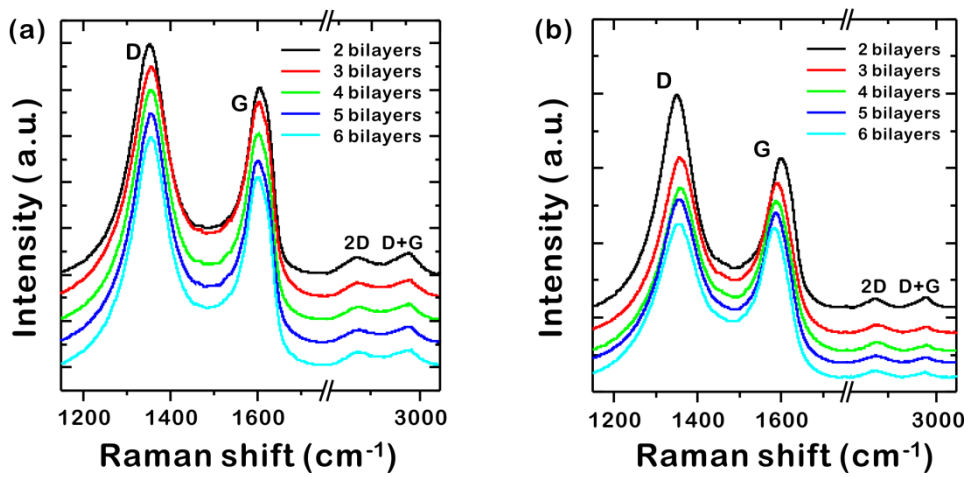


Figure 1-10 Raman spectra of CRGO and TRGO films with various numbers of graphene bilayers.

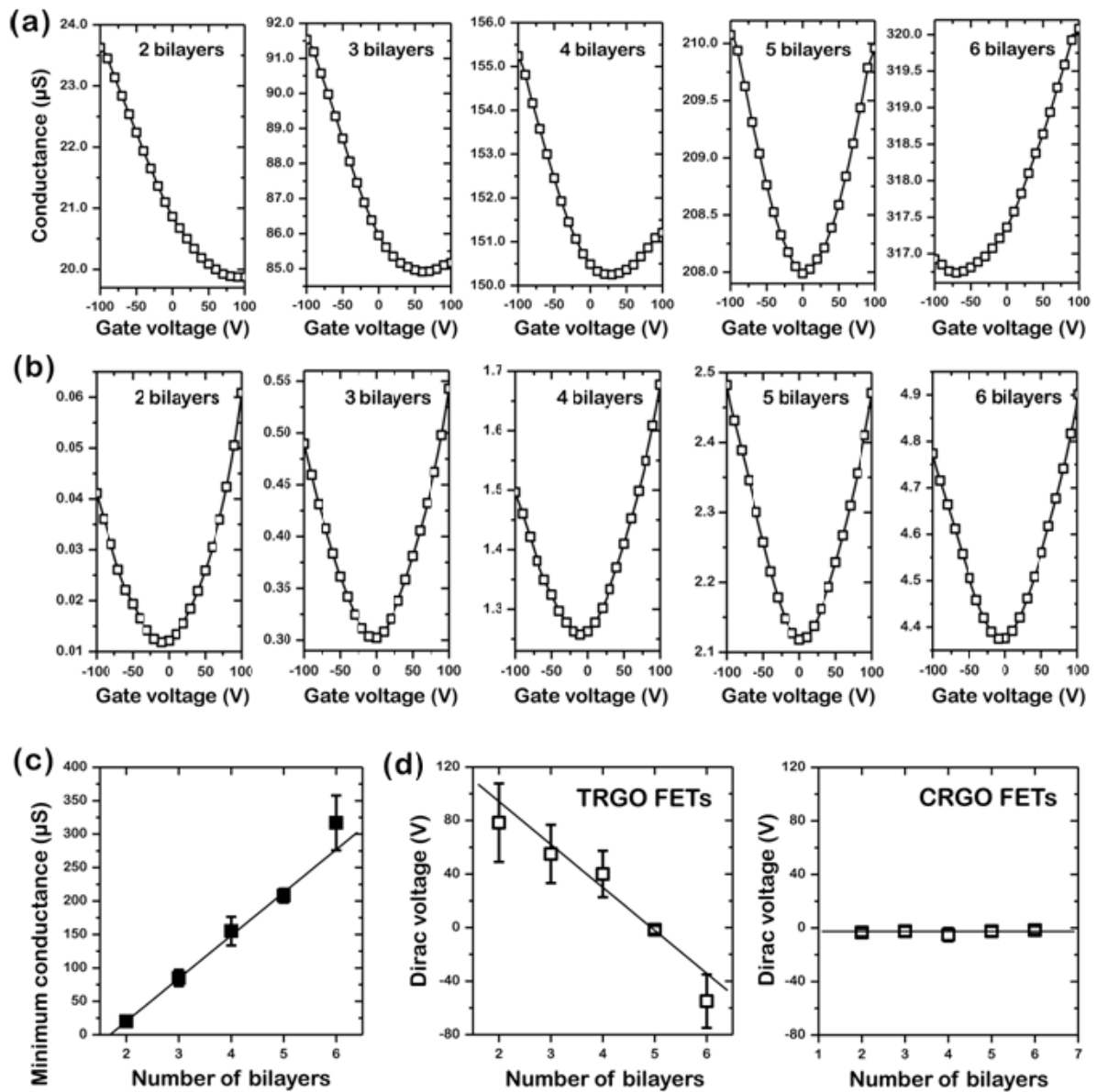


Figure 1-11 Transfer characteristics of (a) TRGO, (b) CRGO FETs with various numbers of graphene bilayers (c) Minimum conductance of TRGO FETs as a function of number of graphene bilayers. (d) Dirac voltage changes in TRGO and CRGO based FETs as a function of number of graphene bilayers.

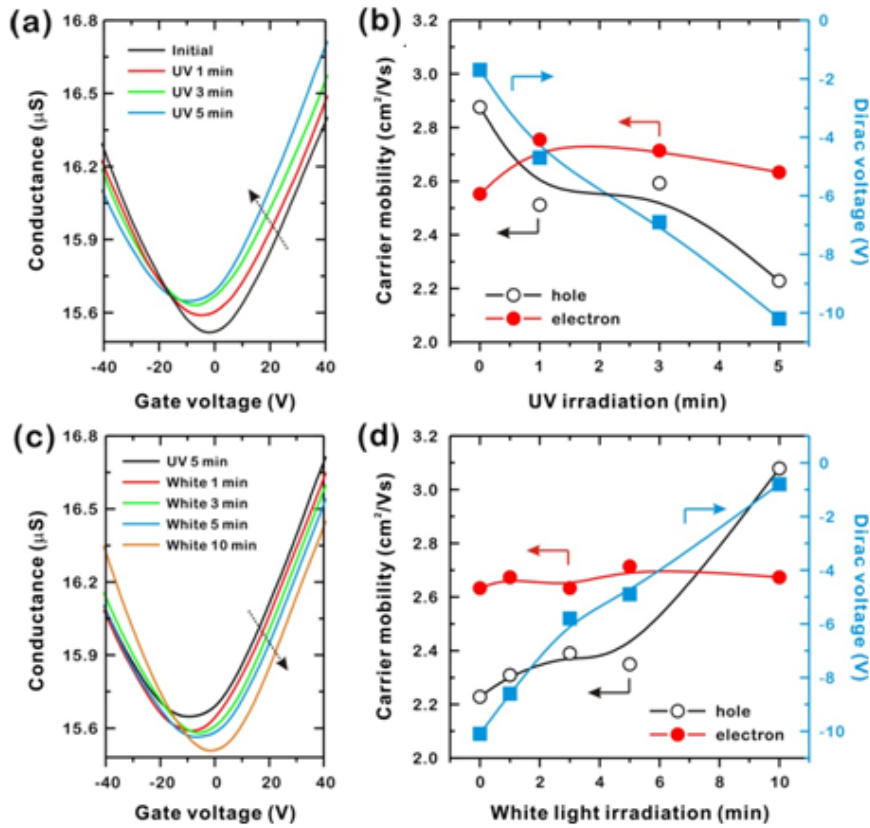


Figure 1-12 Transfer characteristics of the SP functionalized 2-bilayer graphene FETs ($V_D = -0.1$ V) upon (a, b) UV and (c, d) white light irradiation. (b, d) The right panels show the corresponding changes of the carrier mobilities and Dirac voltage as a function of the UV and white light irradiation time.

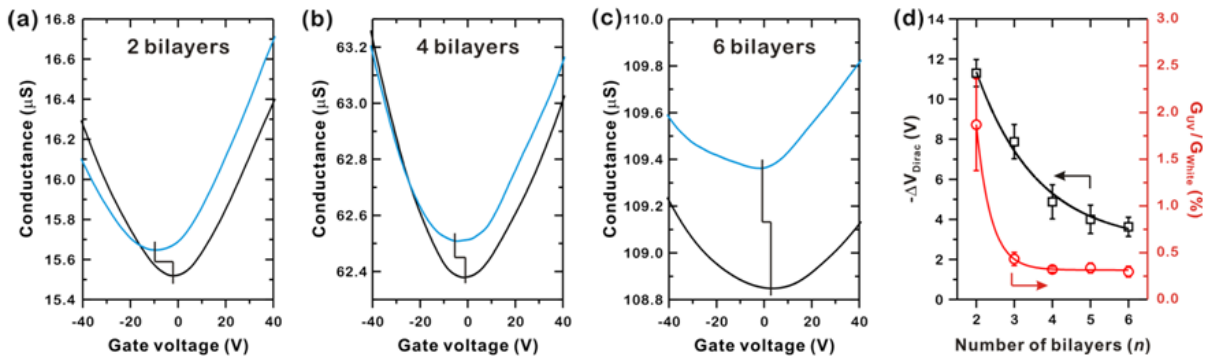


Figure 1-13 (a-c) Transfer characteristics of the SP-functionalized 2, 4, and 6-bilayer graphene FETs ($V_D = -0.1$ V) (black) before and (blue) after UV irradiation for 5 min. (d) Dirac voltage shift ($-\Delta V_{\text{Dirac}}$) and minimum conductance ratio ($G_{\text{UV}}/G_{\text{white}}$) between UV and white light irradiation as a function of the number of bilayers. The lines in (a-c) are included to aid the Dirac voltage shift and conductance changes. All values were reported with three independent measurements.

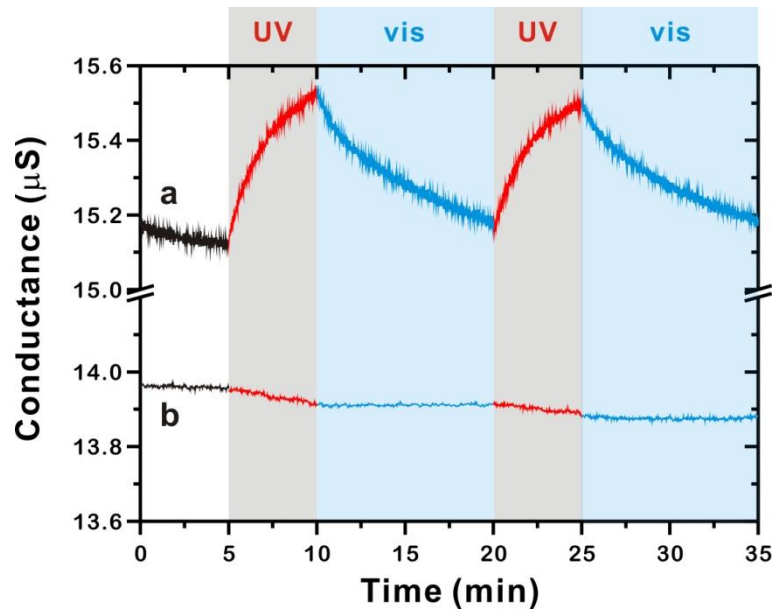


Figure 1-14 Time-course measurements of drain current of (a) SP-functionalized and (b) unmodified 2-bilayer graphene multilayer FET ($V_D = -0.1$ V and $V_G = -5$ V). Alternating irradiation cycles with UV and visible white light were employed during the measurements.

1.5 Summary

In conclusion, we present a facile method of achieving Dirac point control in reduced graphene oxide multilayer FETs that are thermally reduced at high temperature or non-covalently functionalized with a photoresponsive spiropyran derivative. LbL assembly afforded a facile solution-based protocol for controlled assembly of graphene nanosheets. The versatile nature of LbL assembly integrated with the different reduction condition and smart photoresponsive molecules as well. A means of controlling the device performance can be of potential interest in the design of new graphene based electronic devices and sensors.

1.6 References

1. Geim, A. K.;Novoselov, K. S. The Rise of Graphene. *Nat. Mater.* **2007**, *6*, 183-191.
2. Wu, J. S.;Pisula, W.;Mullen, K. Graphenes as Potential Material for Electronics. *Chem. Rev.* **2007**, *107*, 718-747.
3. Kim, K. S.;Zhao, Y.;Jang, H.;Lee, S. Y.;Kim, J. M.;Ahn, J. H.;Kim, P.;Choi, J. Y.;Hong, B. H. Large-Scale Pattern Growth of Graphene Films for Stretchable Transparent Electrodes. *Nature* **2009**, *457*, 706-710.
4. Balandin, A. A.;Ghosh, S.;Bao, W. Z.;Calizo, I.;Teweldebrhan, D.;Miao, F.;Lau, C. N. Superior Thermal Conductivity of Single-Layer Graphene. *Nano Lett.* **2008**, *8*, 902-907.
5. Stankovich, S.;Dikin, D. A.;Dommett, G. H. B.;Kohlhaas, K. M.;Zimney, E. J.;Stach, E. A.;Piner, R. D.;Nguyen, S. T.;Ruoff, R. S. Graphene-Based Composite Materials. *Nature* **2006**, *442*, 282-286.
6. Geim, A. K. Graphene: Status and Prospects. *Science* **2009**, *324*, 1530-1534.
7. Castro Neto, A. H.;Guinea, F.;Peres, N. M. R.;Novoselov, K. S.;Geim, A. K. The Electronic Properties of Graphene. *Rev. Mod. Phys.* **2009**, *81*, 109-162.
8. Morozov, S. V.;Novoselov, K. S.;Katsnelson, M. I.;Schedin, F.;Elias, D. C.;Jaszczak, J. A.;Geim, A. K. Giant Intrinsic Carrier Mobilities in Graphene and Its Bilayer. *Phys. Rev. Lett.* **2008**, *100*, 016602.
9. Novoselov, K. S.;Geim, A. K.;Morozov, S. V.;Jiang, D.;Katsnelson, M. I.;Grigorieva, I. V.;Dubonos, S. V.;Firsov, A. A. Two-Dimensional Gas of Massless Dirac Fermions in Graphene. *Nature* **2005**, *438*, 197-200.
10. Novoselov, K. S.;Jiang, Z.;Zhang, Y.;Morozov, S. V.;Stormer, H. L.;Zeitler, U.;Maan, J. C.;Boebinger, G. S.;Kim, P.;Geim, A. K. Room-Temperature Quantum Hall Effect in Graphene. *Science* **2007**, *315*, 1379-1379.
11. Zhang, Y. B.;Tan, Y. W.;Stormer, H. L.;Kim, P. Experimental Observation of The Quantum Hall Effect and Berry's Phase in Graphene. *Nature* **2005**, *438*, 201-204.
12. Wang, S.;Ang, P. K.;Wang, Z. Q.;Tang, A. L. L.;Thong, J. T. L.;Loh, K. P. High Mobility, Printable, and Solution-Processed Graphene Electronics. *Nano Lett.* **2010**, *10*, 92-98.
13. Palacios, T.;Hsu, A.;Wang, H. Applications of Graphene Devices in RF Communications. *IEEE Comm. Mag.* **2010**, *48*, 122-128.
14. Wang, H.;Nezich, D.;Kong, J.;Palacios, T. Graphene Frequency Multipliers. *IEEE Elec. Dev. Lett.* **2009**, *30*, 547-549.
15. Novoselov, K. S.;Geim, A. K.;Morozov, S. V.;Jiang, D.;Zhang, Y.;Dubonos, S. V.;Grigorieva, I. V.;Firsov, A. A. Electric Field Effect in Atomically Thin Carbon Films. *Science* **2004**, *306*,

- 666-669.
16. Chen, Z. H.;Lin, Y. M.;Rooks, M. J.;Avouris, P. Graphene Nano-Ribbon Electronics. *Phys. E.* **2007**, *40*, 228-232.
 17. Han, M. Y.;Özyilmaz, B.;Zhang, Y.;Kim, P. Energy Band-Gap Engineering of Graphene Nanoribbons. *Phys. Rev. Lett.* **2007**, *98*, 206805.
 18. Li, X. L.;Wang, X. R.;Zhang, L.;Lee, S. W.;Dai, H. J. Chemically Derived, Ultrasoft Graphene Nanoribbon Semiconductors. *Science* **2008**, *319*, 1229-1232.
 19. Zhu, Y.;Tour, J. M. Graphene Nanoribbon Thin Films Using Layer-by-Layer Assembly. *Nano Lett.* **2010**, *10*, 4356-4362.
 20. Li, X. L.;Wang, H. L.;Robinson, J. T.;Sanchez, H.;Diankov, G.;Dai, H. J. Simultaneous Nitrogen Doping and Reduction of Graphene Oxide. *J. Am. Chem. Soc.* **2009**, *131*, 15939-15944.
 21. Lee, B.;Chen, Y.;Duerr, F.;Mastrogiovanni, D.;Garfunkel, E.;Andrei, E. Y.;Podzorov, V. Modification of Electronic Properties of Graphene with Self-Assembled Monolayers. *Nano Lett.* **2010**, *10*, 2427-2432.
 22. Lee, W. H.;Park, J.;Kim, Y.;Kim, K. S.;Hong, B. H.;Cho, K. Control of Graphene Field-Effect Transistors by Interfacial Hydrophobic Self-Assembled Monolayers. *Adv. Mater.* **2011**, *23*, 3460-3464.
 23. Nouchi, R.;Shiraishi, M.;Suzuki, Y. Transfer Characteristics in Graphene Field-Effect Transistors with Co Contacts. *Appl. Phys. Lett.* **2008**, *93*, 152104.
 24. Nouchi, R.;Tanigaki, K. Charge-Density Depinning at Metal Contacts of Graphene Field-Effect Transistors. *Appl. Phys. Lett.* **2010**, *96*, 253503.
 25. Li, H.;Zhang, Q.;Liu, C.;Xu, S. H.;Gao, P. Q. Ambipolar to Unipolar Conversion in Graphene Field-Effect Transistors. *ACS Nano* **2011**, *5*, 3198-3203.
 26. Wang, Y.;Chen, X. H.;Zhong, Y. L.;Zhu, F. R.;Loh, K. P. Large Area, Continuous, Few-Layered Graphene as Anodes in Organic Photovoltaic Devices. *Appl. Phys. Lett.* **2009**, *95*, 063302.
 27. Liu, F.;Choi, J. Y.;Seo, T. S. DNA Mediated Water-Dispersible Graphene Fabrication and Gold Nanoparticle-Graphene Hybrid. *Chem. Comm.* **2010**, *46*, 2844-2846.
 28. Kim, M.;Safron, N. S.;Huang, C. H.;Arnold, M. S.;Gopalan, P. Light-Driven Reversible Modulation of Doping in Graphene. *Nano Lett.* **2012**, *12*, 182-187.
 29. Kroto, H. W.;Allaf, A. W.;Balm, S. P. C60 - Buckminsterfullerene. *Chem. Rev.* **1991**, *91*, 1213-1235.
 30. Baughman, R. H.;Zakhidov, A. A.;de Heer, W. A. Carbon Nanotubes - The Route toward Applications. *Science* **2002**, *297*, 787-792.

31. Kroto, H. W.;Heath, J. R.;O'Brien, S. C.;Curl, R. F.;Smalley, R. E. C-60 - Buckminsterfullerene. *Nature* **1985**, *318*, 162-163.
32. Iijima, S. Helical Microtubules of Graphitic Carbon. *Nature* **1991**, *354*, 56-58.
33. Vigolo, B.;Penicaud, A.;Coulon, C.;Sauder, C.;Pailler, R.;Journet, C.;Bernier, P.;Poulin, P. Macroscopic Fibers and Ribbons of Oriented Carbon Nanotubes. *Science* **2000**, *290*, 1331-1334.
34. Bandyopadhyaya, R.;Nativ-Roth, E.;Regev, O.;Yerushalmi-Rozen, R. Stabilization of Individual Carbon Nanotubes in Aqueous Solutions. *Nano Lett.* **2002**, *2*, 25-28.
35. Avouris, P.;Chen, Z. H.;Perebeinos, V. Carbon-Based Electronics. *Nat. Nanotechnol.* **2007**, *2*, 605-615.
36. Li, X. S.;Cai, W. W.;An, J. H.;Kim, S.;Nah, J.;Yang, D. X.;Piner, R.;Velamakanni, A.;Jung, I.;Tutuc, E.;Banerjee, S. K.;Colombo, L.;Ruoff, R. S. Large-Area Synthesis of High-Quality and Uniform Graphene Films on Copper Foils. *Science* **2009**, *324*, 1312-1314.
37. Berger, C.;Song, Z. M.;Li, X. B.;Wu, X. S.;Brown, N.;Naud, C.;Mayou, D.;Li, T. B.;Hass, J.;Marchenkov, A. N.;Conrad, E. H.;First, P. N.;de Heer, W. A. Electronic Confinement and Coherence in Patterned Epitaxial Graphene. *Science* **2006**, *312*, 1191-1196.
38. Ohta, T.;Bostwick, A.;Seyller, T.;Horn, K.;Rotenberg, E. Controlling The Electronic Structure of Bilayer Graphene. *Science* **2006**, *313*, 951-954.
39. Hernandez, Y.;Nicolosi, V.;Lotya, M.;Blighe, F. M.;Sun, Z. Y.;De, S.;McGovern, I. T.;Holland, B.;Byrne, M.;Gun'ko, Y. K.;Boland, J. J.;Niraj, P.;Duesberg, G.;Krishnamurthy, S.;Goodhue, R.;Hutchison, J.;Scardaci, V.;Ferrari, A. C.;Coleman, J. N. High-Yield Production of Graphene by Liquid-Phase Exfoliation of Graphite. *Nat. Nanotechnol.* **2008**, *3*, 563-568.
40. Li, D.;Muller, M. B.;Gilje, S.;Kaner, R. B.;Wallace, G. G. Processable Aqueous Dispersions of Graphene Nanosheets. *Nat. Nanotechnol.* **2008**, *3*, 101-105.
41. Stankovich, S.;Dikin, D. A.;Piner, R. D.;Kohlhaas, K. A.;Kleinhammes, A.;Jia, Y.;Wu, Y.;Nguyen, S. T.;Ruoff, R. S. Synthesis of Graphene-Based Nanosheets via Chemical Reduction of Exfoliated Graphite Oxide. *Carbon* **2007**, *45*, 1558-1565.
42. Brodie, B. C. On The Atomic Weight of Graphite. *Philos. Trans. R. Soc. London* **1859**, *149*, 249-259.
43. Staudenmaier, L. Verfahren Zur Darstellung Der Graphitsäure. *Ber. Dtsch. Chem. Ges.* **2006**, *31*, 1481-1487.
44. Hummers, W. S.;Offeman, R. E. Preparation of Graphitic Oxide. *J. Am. Chem. Soc.* **1958**, *80*, 1339-1339.
45. Dreyer, D. R.;Park, S.;Bielawski, C. W.;Ruoff, R. S. The Chemistry of Graphene Oxide.

- Chem. Soc. Rev.* **2010**, *39*, 228-240.
46. Becerril, H. A.;Mao, J.;Liu, Z.;Stoltenberg, R. M.;Bao, Z.;Chen, Y. Evaluation of Solution-Processed Reduced Graphene Oxide Films as Transparent Conductors. *ACS Nano* **2008**, *2*, 463-470.
 47. Iler, R. K. Multilayers of Colloidal Particles. *J. Colloid Interf. Sci.* **1966**, *21*, 569-670.
 48. Decher, G. Fuzzy Nanoassemblies: Toward Layered Polymeric Multicomposites. *Science* **1997**, *277*, 1232-1237.
 49. Caruso, F.;Caruso, R. A.;Mohwald, H. Nanoengineering of Inorganic and Hybrid Hollow Spheres by Colloidal Templating. *Science* **1998**, *282*, 1111-1114.
 50. Hong, J.;Han, J. Y.;Yoon, H.;Joo, P.;Lee, T.;Seo, E.;Char, K.;Kim, B. S. Carbon-Based Layer-by-Layer Nanostructures: From Films to Hollow Capsules. *Nanoscale* **2011**, *3*, 4515-4531.
 51. Irie, M. Diarylethenes for Memories and Switches. *Chem. Rev.* **2000**, *100*, 1685-1716.
 52. Natansohn, A.;Rochon, P. Photoinduced Motions in Azo-Containing Polymers. *Chem. Rev.* **2002**, *102*, 4139-4175.
 53. Raymo, F. M.;Tomasulo, M. Electron and Energy Transfer Modulation with Photochromic Switches. *Chem. Soc. Rev.* **2005**, *34*, 327-336.
 54. Raymo, F. M.;Giordani, S. Signal Processing at The Molecular Level. *J. Am. Chem. Soc.* **2001**, *123*, 4651-4652.
 55. Berkovic, G.;Krongauz, V.;Weiss, V. Spiropyrans and Spirooxazines for Memories and Switches. *Chem. Rev.* **2000**, *100*, 1741-1753.
 56. Guo, X. F.;Huang, L. M.;O'Brien, S.;Kim, P.;Nuckolls, C. Directing and Sensing Changes in Molecular Conformation on Individual Carbon Nanotube Field Effect Transistors. *J. Am. Chem. Soc.* **2005**, *127*, 15045-15047.
 57. Kovtyukhova, N. I.;Ollivier, P. J.;Martin, B. R.;Mallouk, T. E.;Chizhik, S. A.;Buzaneva, E. V.;Gorchinskiy, A. D. Layer-by-Layer Assembly of Ultrathin Composite Films from Micron-Sized Graphite Oxide Sheets and Polycations. *Chem. Mater.* **1999**, *11*, 771-778.
 58. Lee, D. W.;Hong, T. K.;Kang, D.;Lee, J.;Heo, M.;Kim, J. Y.;Kim, B. S.;Shin, H. S. Highly Controllable Transparent and Conducting Thin Films Using Layer-by-Layer Assembly of Oppositely Charged Reduced Graphene Oxides. *J. Mater. Chem.* **2011**, *21*, 3438-3442.
 59. Ramanathan, T.;Fisher, F. T.;Ruoff, R. S.;Brinson, L. C. Amino-Functionalized Carbon Nanotubes for Binding to Polymers and Biological Systems. *Chem. Mater.* **2005**, *17*, 1290-1295.
 60. Zhang, C. H.;Fu, L.;Liu, N.;Liu, M. H.;Wang, Y. Y.;Liu, Z. F. Synthesis of Nitrogen-Doped Graphene Using Embedded Carbon and Nitrogen Sources. *Adv. Mater.* **2011**, *23*, 1020-1024.

61. Sheng, Z. H.;Shao, L.;Chen, J. J.;Bao, W. J.;Wang, F. B.;Xia, X. H. Catalyst-Free Synthesis of Nitrogen-Doped Graphene via Thermal Annealing Graphite Oxide with Melamine and Its Excellent Electrocatalysis. *ACS Nano* **2011**, *5*, 4350-4358.
62. Hong, T. K.;Lee, D. W.;Choi, H. J.;Shin, H. S.;Kim, B. S. Transparent, Flexible Conducting Hybrid Multi layer Thin Films of Multiwalled Carbon Nanotubes with Graphene Nanosheets. *ACS Nano* **2010**, *4*, 3861-3868.
63. Shin, H. J.;Kim, S. M.;Yoon, S. M.;Benayad, A.;Kim, K. K.;Kim, S. J.;Park, H. K.;Choi, J. Y.;Lee, Y. H. Tailoring Electronic Structures of Carbon Nanotubes by Solvent with Electron-Donating and -Withdrawing Groups. *J. Am. Chem. Soc.* **2008**, *130*, 2062-2066.
64. Voggu, R.;Rout, C. S.;Franklin, A. D.;Fisher, T. S.;Rao, C. N. R. Extraordinary Sensitivity of The Electronic Structure and Properties of Single-Walled Carbon Nanotubes to Molecular Charge-Transfer. *J. Phys. Chem. C* **2008**, *112*, 13053-13056.
65. Guo, B. D.;Liu, Q. A.;Chen, E. D.;Zhu, H. W.;Fang, L. A.;Gong, J. R. Controllable N-Doping of Graphene. *Nano Lett.* **2010**, *10*, 4975-4980.
66. Lin, Y. C.;Lin, C. Y.;Chiu, P. W. Controllable Graphene N-Doping with Ammonia Plasma. *Appl. Phys. Lett.* **2010**, *96*, 133110.
67. Das, A.;Pisana, S.;Chakraborty, B.;Piscanec, S.;Saha, S. K.;Waghmare, U. V.;Novoselov, K. S.;Krishnamurthy, H. R.;Geim, A. K.;Ferrari, A. C.;Sood, A. K. Monitoring Dopants by Raman Scattering in An Electrochemically Top-Gated Graphene Transistor. *Nat. Nanotechnol.* **2008**, *3*, 210-215.
68. Liu, L.;Ryu, S. M.;Tomasik, M. R.;Stolyarova, E.;Jung, N.;Hybertsen, M. S.;Steigerwald, M. L.;Brus, L. E.;Flynn, G. W. Graphene Oxidation: Thickness-Dependent Etching and Strong Chemical Doping. *Nano Lett.* **2008**, *8*, 1965-1970.
69. Wohl, C. J.;Kuciauskas, D. Excited-State Dynamics of Spiropyran-Derived Merocyanine Isomers. *J. Phys. Chem. B* **2005**, *109*, 22186-22191.
70. Yan, Z.;Sun, Z. Z.;Lu, W.;Yao, J.;Zhu, Y.;Tour, J. M. Controlled Modulation of Electronic Properties of Graphene by Self-Assembled Monolayers on SiO₂ Substrates. *ACS Nano* **2011**, *5*, 1535-1540.
71. Chen, F.;Xia, J. L.;Ferry, D. K.;Tao, N. J. Dielectric Screening Enhanced Performance in Graphene FET. *Nano Lett.* **2009**, *9*, 2571-2574.

Chapter 2. Possibilities of 2D Layered Transition Metal Dichalcogenide Multilayers by Using Layer-by-Layer Assembly

2.1 Abstract

Since graphene was focused on its novel properties, two-dimensional crystal of metal dichalcogenides also has been highlighted for hydrogen evolution catalysts and optoelectronics as well. Layered transition metal dichalcogenide monolayer is a photoluminescent direct gap semiconductor in striking contrast to its bulk counterpart. Here, we report multilayer structural properties of chemically exfoliated layered transition metal dichalcogenides by using layer-by-layers assembly with different number of polymer interlayer between layered transition metal dichalcogenides sheets. This method results in improvement of potential optoelectronic properties with exhibition of prominent photoluminescence of layered transition metal dichalcogenides, especially MoS₂.

2.2 Introduction

Layered transition metal dichalcogenides (LTMDs) are extensively used as a solid state lubricant and catalyst for hydrodesulfurization and hydrogen evolution (**Figure 2-1**).^{6,9,76} Since a two-dimensional carbon lattice structured material, graphene, successfully isolated from graphite, two-dimensional materials have been highlighted because their novel mechanical, chemical, and electrical properties for diverse applications.^{1,2,10-13} Similar to graphene, exfoliated LTMDs such as molybdenum disulfide and tungsten disulfide represent wide range applicable materials for electronics and hydrogen evolution catalysts.^{9,77-82} LTMDs can be easily exfoliated to individual monolayers by “scotch tape method” used to graphene⁸³ and “lithium intercalation method”.⁸⁴ The exfoliated two-dimensional crystals of LTMDs are direct band gap semiconductor.^{9,82,85-87} Photoluminescence (PL) of the LTMDs indicates variable potentials for and photo-induced hydrogen evolution catalysts and optoelectronics (**Figure 2-2**).^{7,9} With thickness decreases, the band gap of LTMDs increases owing to quantum confinement.⁹ In addition, the nature of the band gap changes from indirect to direct when the thickness reaches a single layer.⁹

Although mechanically exfoliated LTMDs have few defects, large scale production is significant in industry, so that the solution process is a strongly recommended method. Coleman and co-workers proposed solvent assisted exfoliation of two-dimensional LTMDs from bulk phase in various organic solvent by ultrasonication (**Figure 2-3**)⁸; however, a lack of monolayered productions was observed in this method. Lithium intercalated MoS₂ (Li_xMoS₂) has been well known procedure to exfoliate bulk phase MoS₂ into the negatively charged monolayers in water since Morrison and co-workers showed the result.⁸⁴ Also, Chhowalla and co-workers demonstrated chemically exfoliated large scale MoS₂ and its possibilities of optoelectronic applications after mild annealing process (**Figure 2-4**).⁹

Layer-by-layer (LbL) assembly of two-dimensional materials such as metal oxide and graphene has been studied to design those specific morphologies, and the LbL assembled composites has been demonstrated to improve mechanical, electrical, and electrochemical properties.^{88,89} In 1998, Mallouk and co-workers presented possibility of multilayer stacking of MoS₂ (or SnS₂) by using LbL assembly with different positively charged polyelectrolytes, and they analyzed thickness increase and surface morphology of MoS₂ (or SnS₂) multilayer films.⁹⁰

2.2.1 Solution process of layered transition metal dichalcogenides

For large scale production of LTMDs to utilize many applications, either synthesis or exfoliation in solution is inevitable. Between two representative methods, a solution process is the suggested processing route for low cost and easy process.^{8,9} For example, chemical vapor deposition (CVD)

growth methods to synthesize LTMDs at high temperature with sensitive control over 800 °C are costly synthesis manners due to setting up of specially designed furnace and consuming high electricity.⁹¹ In contrast, a lithium intercalation between layers of LTMDs^{9,84} and a solvent assist exfoliation method with sonication have been well known simple solution processes.⁸ Practically, after lithium intercalation, the phase transformations of LTMD occur.^{9,92,93} For example, during the reaction with lithium, MoS₂ trigonal prismatic (2H-MoS₂) changes to octahedral (1T-MoS₂) phase; however the exfoliated LTMDs in various organic solvent with sonication possibly maintain those nature properties.⁸ Unfortunately, a tiny amount of monolayers can be collected in organic solvents with sonication method. This is a crucial drawback to employ LTMDs to PL related applications.⁹

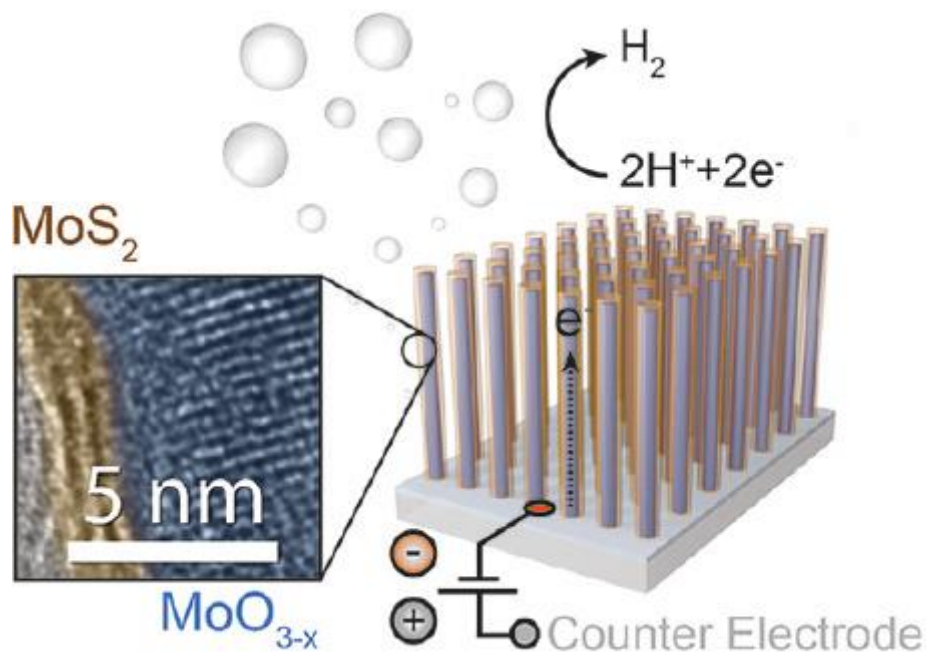


Figure 2-1 illustrations of MoO₃-MoS₂ hydrogen evolution catalyst.⁶ (Chen et al., *Nano Lett.* **2011**, *11*, 4168)

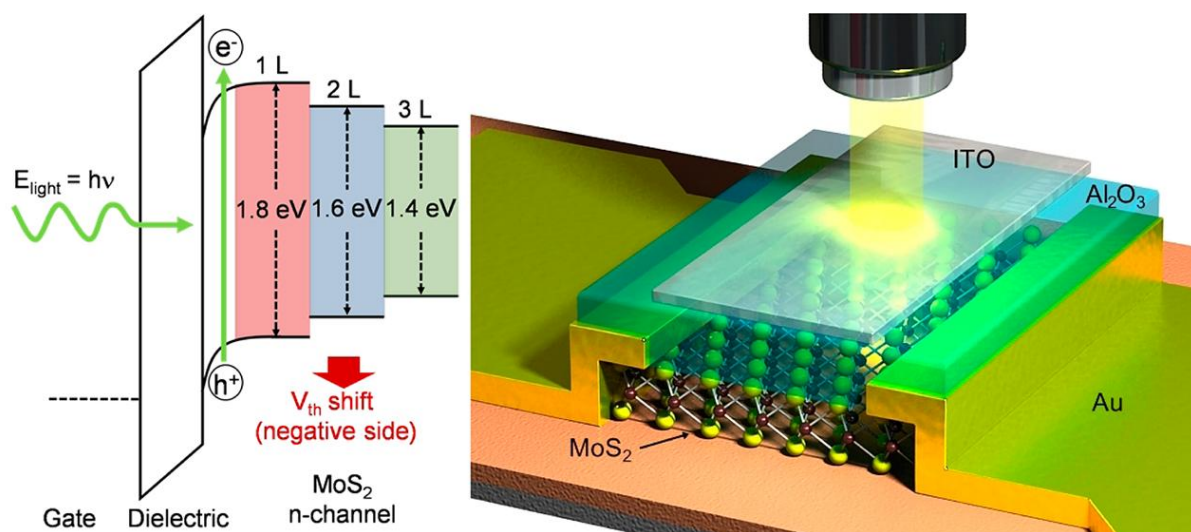


Figure 2-2 illustrations of phototransistor using MoS₂ thin films.⁷ (Lee et al., *Nano Lett.* **2012**, *12*, 3695)

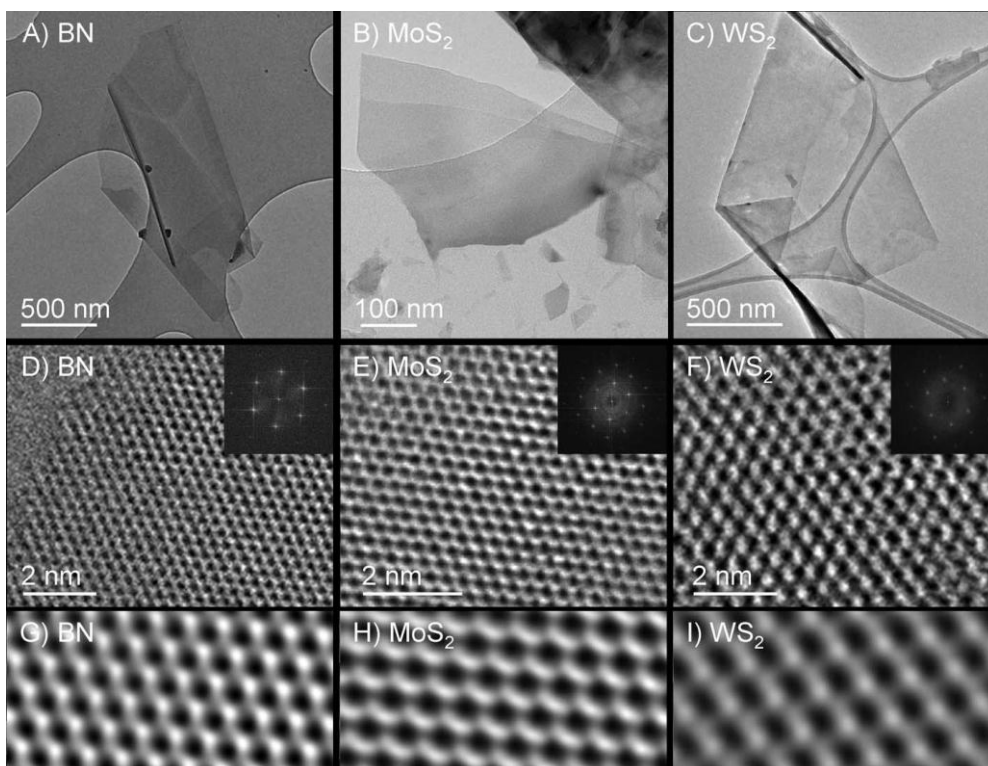


Figure 2-3 TEM images of exfoliated nanosheets to the solvent assist method.⁸ (A to C) Low resolution TEM images of flakes of BN, MoS₂, and WS₂, respectively. (D to F) High-resolution TEM images of BN, MoS₂, and WS₂ monolayers (Insets) Fast Fourier transforms of the images. (G to I) Butterworth-filtered images of sections of the images in (D) to (F) (Coleman et al., *Science* **2011**, 331, 568)

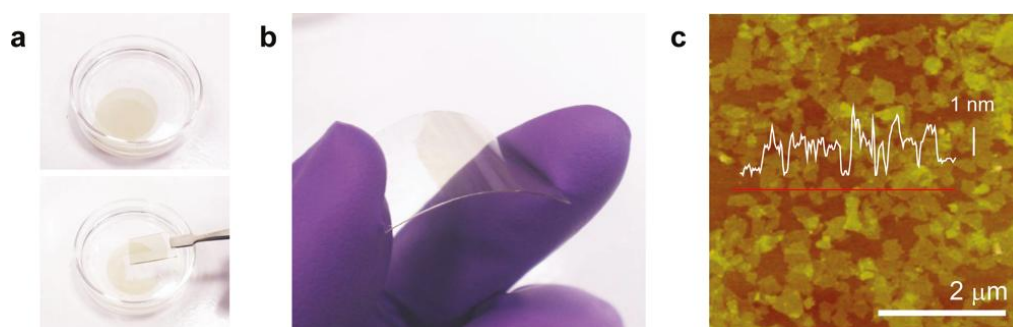
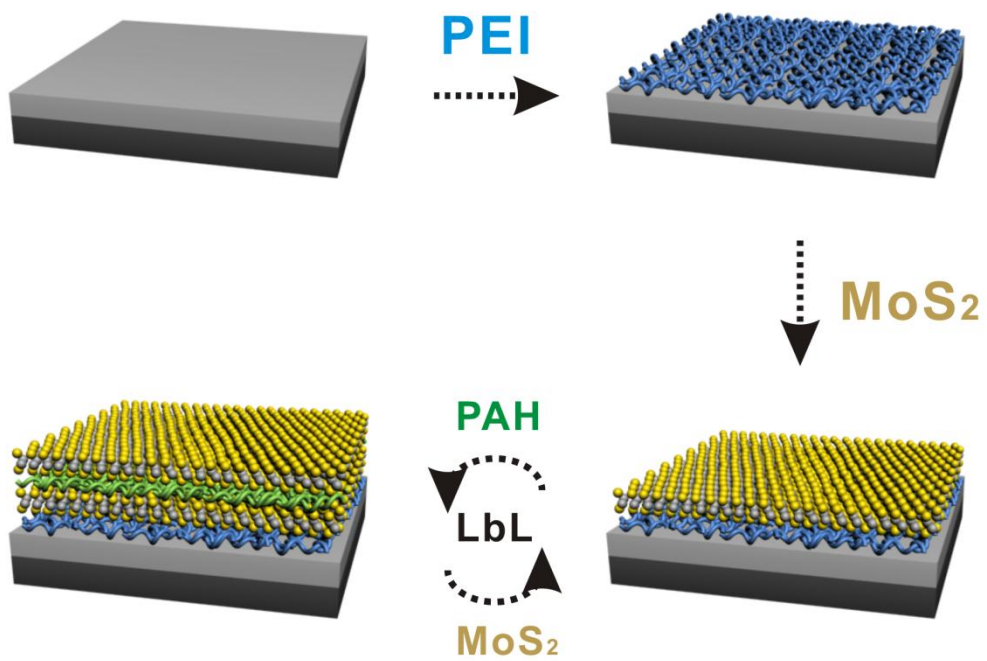


Figure 2-4 Films of exfoliated MoS₂ nanosheets *via* lithium intercalation.⁹ (a) Photograph of MoS₂ film floating on water (top panel) and deposited on glass (bottom panel) (b) Photograph of an asdeposited thin film of MoS₂ on flexible PET. The films in (a) and (b) are approximately 5 nm thick (c) AFM image of an ultrathin film with an average thickness of 1.3 nm. The film consists of regions that are covered by monolayers and others that are slightly thicker due to overlap between individual sheets. Height profile along the red line is overlaid on the image. (Eda et al., *Nano Lett.* **2011**, 11, 5111)



Scheme 2-1 Schematic representation of layer-by-layer assembled MoS₂ multilayer.

2.3 Experimental

2.3.1 Preparation of MoS₂ solutions

Lithium intercalation technique is well introduced in Morrison's paper.⁸⁴ Briefly, lithium intercalated MoS₂ was achieved by immersing 400 mg of each bulk phase crystals in 4 mL n-butyllithium solution with inert inert gas for 2 days. The LixMoS₂ was washed with hexane to remove residues and dried under vacuum. The dried LixMoS₂ was exfoliated by ultrasonication in deionized water. The mixture was purified to cycles of centrifugations.

2.3.2 Fabrications of MoS₂ multilayer

MoS₂ films were basically fabricated by using LbL assembly to isolate single and few layerd MoS₂ sheets. Polyethylenimine (PEI) was used to a first layer for the high quality build-up, and the other positively charged polyallylamine hydrochloride (PAH) was coated onto negatively charged MoS₂ surfaces which already adhered on PEI.

As a consequence for the film fabrication, the multilayer films were by repeatedly dipping with spin onto a planar SiO₂/Si substrate or a quartz slide for the multilayer in an architecture of (PEI/MoS₂)₁/(PAH/ MoS₂)_n ($1+n$ = number of bilayer, typically $n = 1-3$), and all fabricated samples were annealed at 300 °C to restore their semiconducting properties.

2.4 Results and Discussion

The scanning electron microscopy (SEM) images of MoS₂ 1-4 bilayer (BL) films are shown well growth morphology (**Figure 2-5**). Few layered flakes are observed at all images owing to difficulties of solution process to purifying monolayer. Initial MoS₂ layer display not fully covered surface due to the electrostatic repulsion among the sheets as often observed in initial few layers of polyelectrolyte-based LbL systems. Possibly, exfoliated 2D materials entirely coat on polyelectrolyte, however, many overlapped sheets occur on densely packed surface. The overlapped sheets can interrupt PL generation with changing band gap for optoelectronics.⁹ Interestingly, as increase number of MoS₂ layers, the sheets are growth to the vertical direction on initially coated MoS₂ layers.

To study the influence of thermal annealing, we have employed X-ray photoemission spectroscopy (XPS) analysis to confirm phase transformations of 1T- to 2H- MoS₂ on the PEI coated surface. Conducting behaviors and the quenching of 1T-MoS₂ above 100 °C are well known properties.⁹ **Figure 2-6a** shows a survey XPS spectrum of 1 BL film. The survey peak is shown not only molybdenum and sulfur from MoS₂, but also carbon, and nitrogen from the layered polymers without any unexpected elements. The high resolution XPS spectra (**Figure 2-6b and c**) demonstrate the 2H-MoS₂ conformation after mild thermal treatments. The Mo spectrum consist of peaks at around 229.7 and 232.9 eV that correspond to Mo3d_{5/2} and Mo3d_{3/2} components of 2H-MoS₂, respectively.^{9,94} Similarly, in the S spectrum, additional peaks are found besides the known doublet peaks of 2H-MoS₂, S2p_{3/2}, and 2p_{1/2}, which appear at 162.5 and 163.4 eV respectively. It is important to note the absence of a prominent peak at 236 eV, which indicates to oxidation of molybdenum.⁹

Raman spectroscopy is the most direct and nondestructive technique to confirm the layered structure of LTMDs. Recent studies reported that the position of E¹_{2g} and A_{1g} peaks depends on the number of monolayers.^{9,91,95} For mechanically exfoliated MoS₂, A_{1g} peak shifted from 407 cm⁻¹ for bulk material to 403 cm⁻¹ for a monolayer, and E¹_{2g} peak changed from 382 and 384 cm⁻¹ for bulk and monolayer MoS₂, respectively.⁹⁵ Similarly, in CVD growth MoS₂ case, A_{1g} peak moved from 407 cm⁻¹ for bulk material to 402 cm⁻¹ for a monolayer, and E¹_{2g} peak changed from 382 cm⁻¹ for bulk to single at 386 cm⁻¹.⁹¹ Moreover, equally exfoliated MoS₂ sheet as our work using lithium intercalation method, Chhowalla and co-workers have shown that raman shift of E¹_{2g} and A_{1g} peaks at around 382 cm⁻¹ and 405 cm⁻¹, respectively, even they displayed peak shift from thin to thick layered MoS₂ films.⁹ Interestingly, in our measured raman spectra with number of bilayers (**Figure 2-7a-d**), as increase number of bilayers, height of normalized raman intensity based on the Si 1st order peak (**Figure 2-7e**) and integrated intensity (**Figure 2-7f**) are linearly improved with a tiny of peak shifts. E¹_{2g} and A_{1g} peak positions are 382.9 cm⁻¹ and 406.3 cm⁻¹, respectively (**Figure 2-7g**). This indicates that polymer layers well isolate each MoS₂ sheet.

The UV/vis absorption spectra (**Figure 2-8a and b**) show consistently increased absorbance as number of bilayers increase. With annealing process, merging and growing of MoS₂ excitonic features are already demonstrated. Arising from K point of the Brillouin zone between 600 nm and 700 nm was shown at previous studied. **Figure 2-8b** displays the broad peaks at 610 nm, 660 nm for minor and major emission spectra, respectively.⁹

The PL of MoS₂ thin films are superior properties for optoelectronics. The gradual PL quenching with film thickness is in contrast to that in mechanically exfoliated MoS₂ where the quantum yield drops quickly from monolayer to bilayer.⁸² Moreover, in previous study which used well exfoliated MoS₂ by lithium intercalation method explained the fact that there may be monolayered regions within the multi-layered films, and weak interlayer coupling between the restacked MoS₂ sheets due to rotational stacking disorder as suggested by Raman analysis could be responsible for the gradual decrease in PL.⁹ However, interestingly, the normalized intensity (**Figure 2-9a-d**) and area (**Figure 2-9e**) of PL spectra of LbL assembled 1-4 BL MoS₂ multilayer films are improved as number of bilayers increase. Major emission peak around 660 nm (≈ 1.88 eV) and minor band peak around 610 nm (≈ 2.03 eV) with carbon expected peak detected. Even initially coated MoS₂ sheets seem to not monolayered film, we confirm that the polymer interlayer possibly isolate between MoS₂ sheets in LbL assembly system for optoelectronic applications.

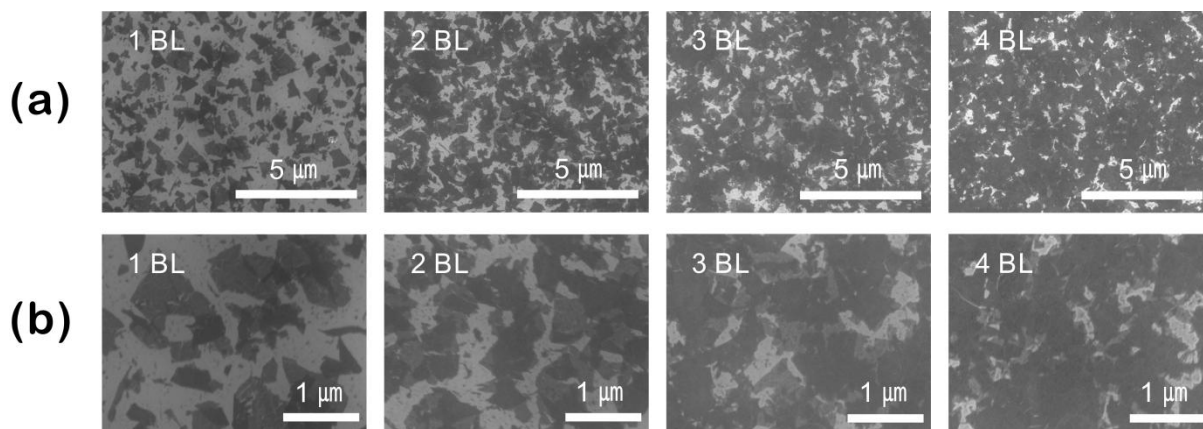


Figure 2-5 Low (a) and high (b) magnified SEM images of MoS₂ multilayer films with various numbers of bilayers.

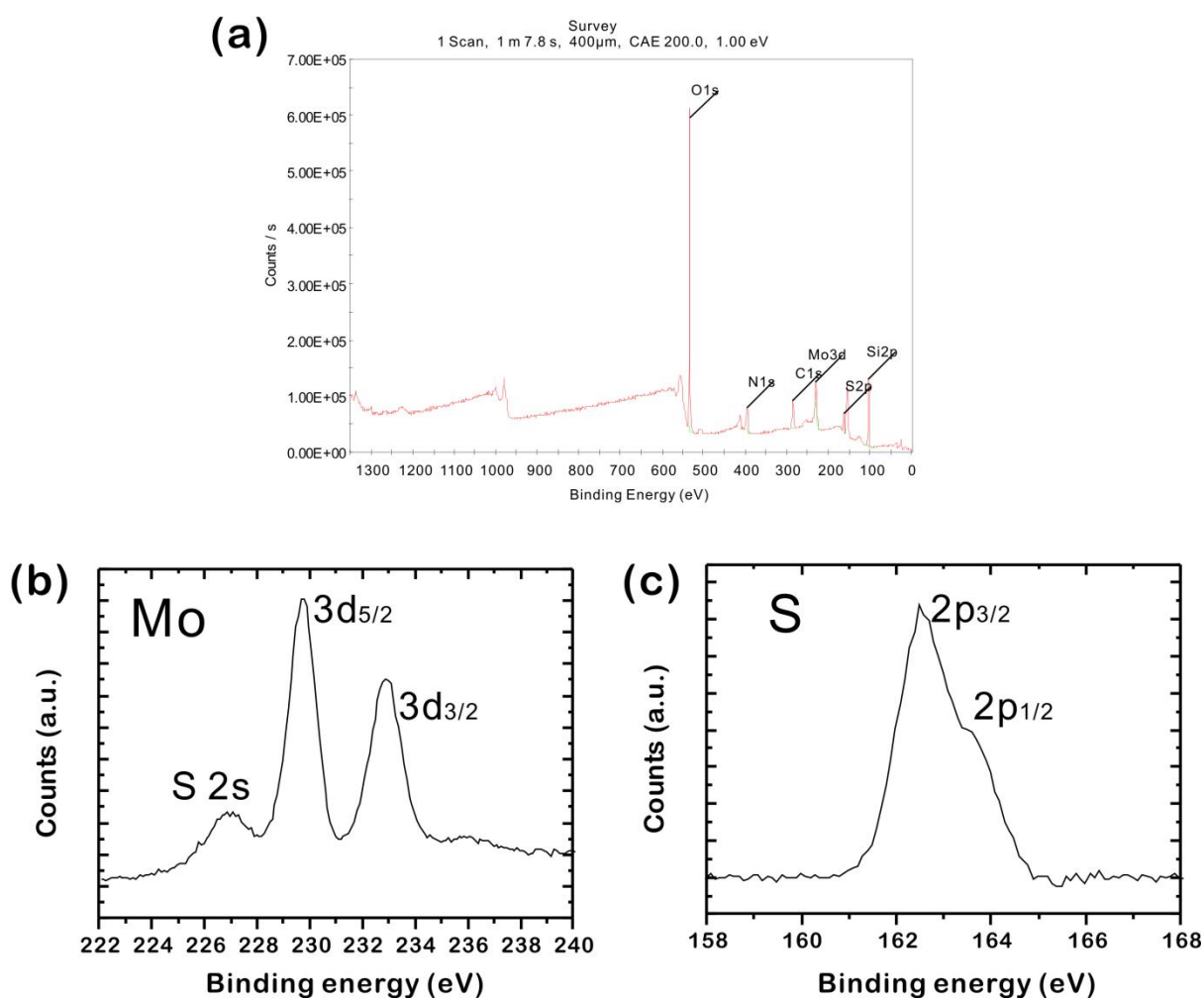


Figure 2-6 XPS analysis of the 1 BL MoS₂ film on SiO₂/Si wafer (a) survey scan (b) Mo (C) S.

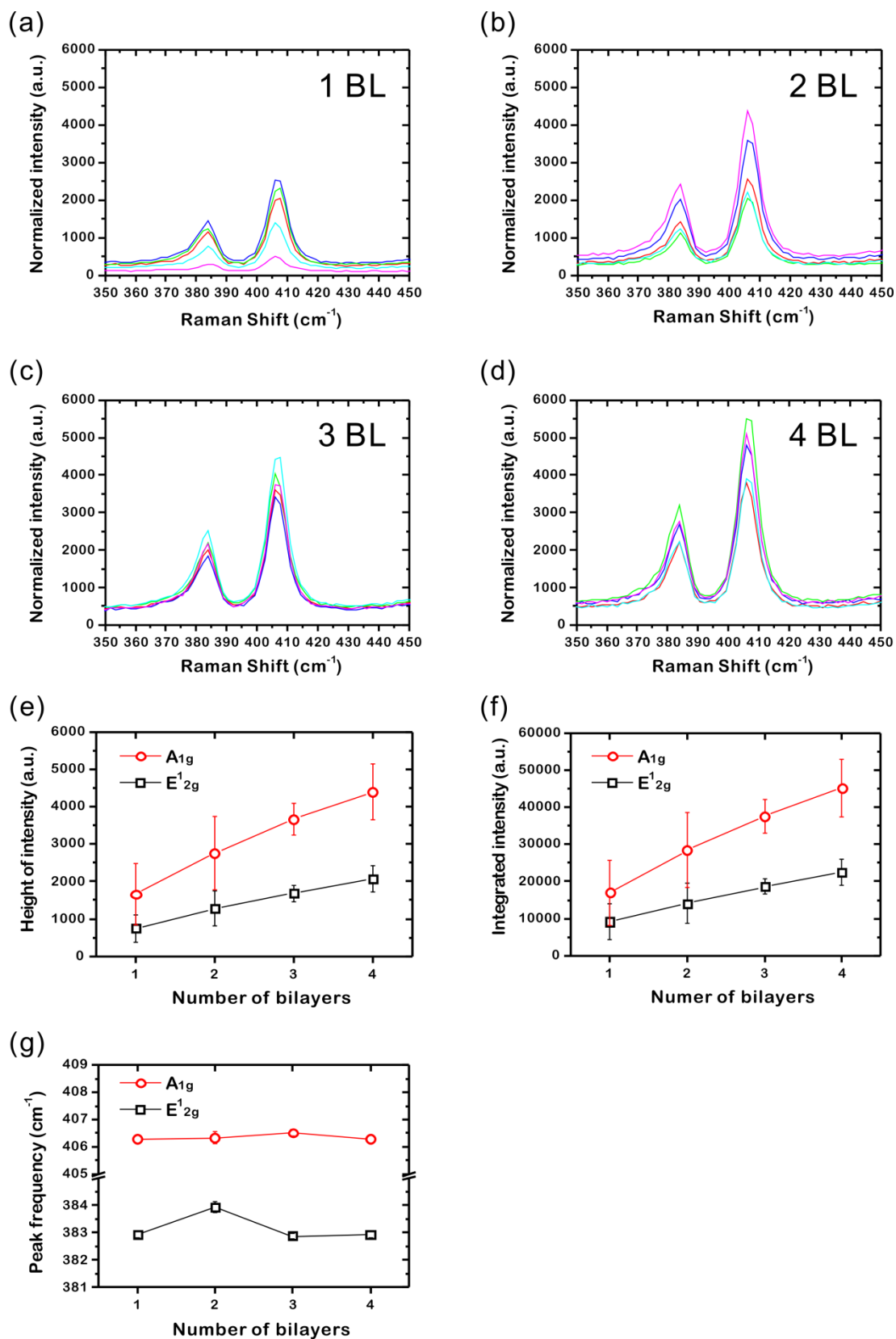


Figure 2-7 (a - d) Raman spectra of annealed MoS₂ thin films (e) height of intensity, (f) integrated intensity, and (g) peak frequency with different number of bilayers.

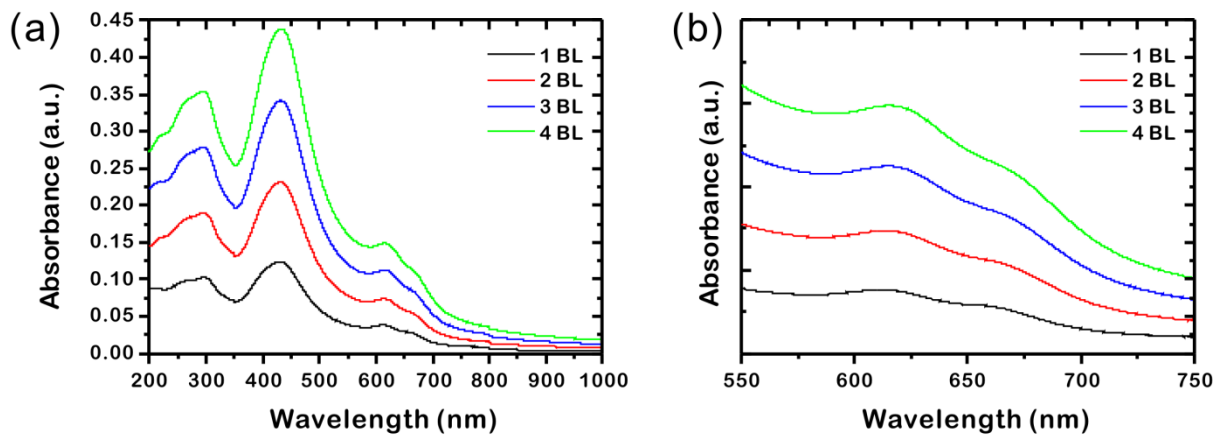


Figure 2-8 UV/vis absorbance spectra of following different numbers of MoS₂ bilayers on quartz substrates (a) Low and (b) high magnified.

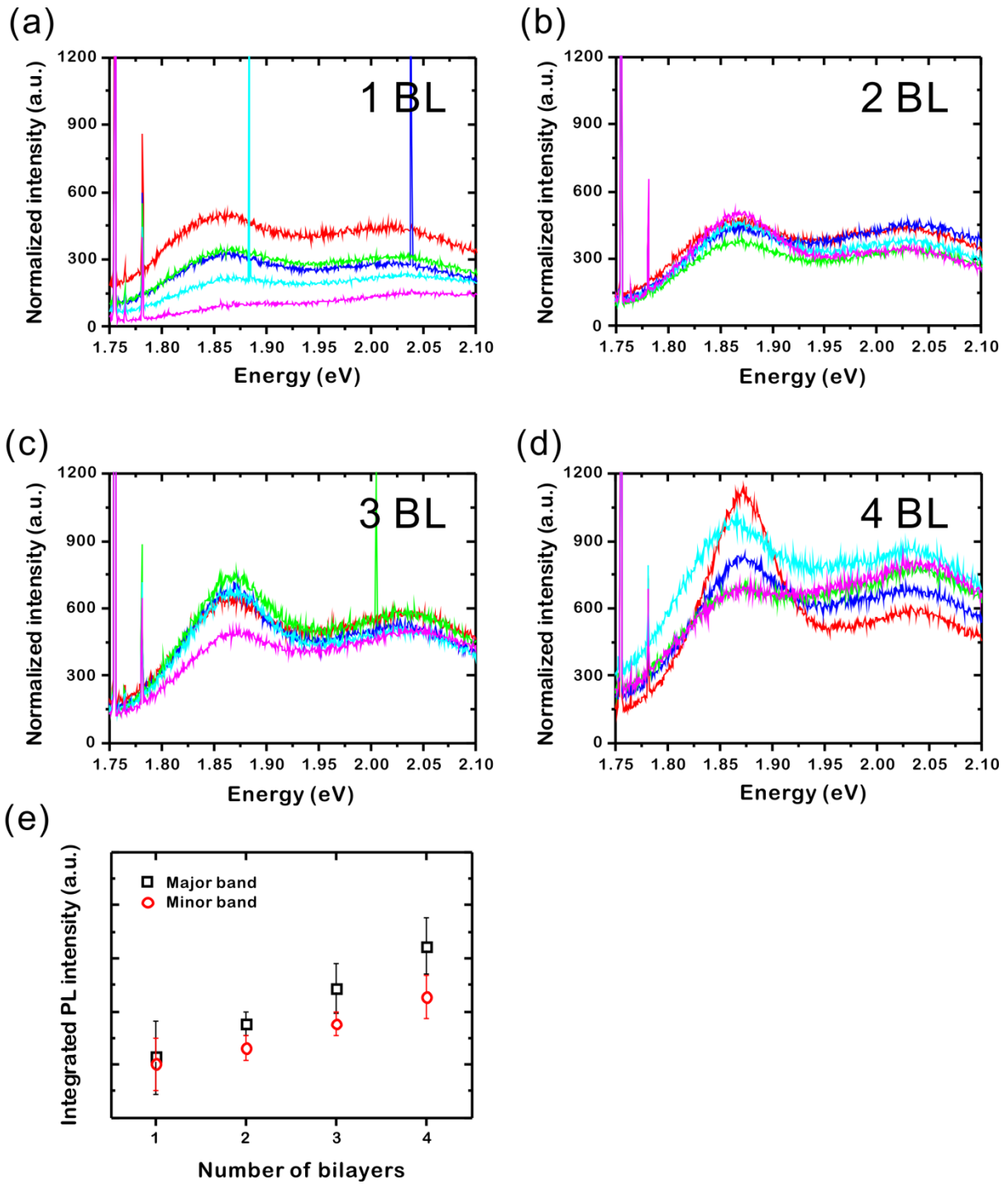


Figure 2-9. Normalized PL spectra and integrated PL intensity differences of MoS₂ multilayer films with different numbers of bilayers.

2.4 Summary

In conclusion, we find that PL of MoS₂ multilayers are gradually improved without any other property changes as number of bilayer increase. This is because of the critical roles of polymer blocks to prevent quenching of direct band gap from a MoS₂ monolayer. The discovery is a promising route for large scale production with solution-based process and development of optoelectronics and photo-induced hydrogen evolution applications of two-dimensional LTMDs with LbL assembly.

2.5 References

1. Eda, G.; Yamaguchi, H.; Voiry, D.; Fujita, T.; Chen, M. W.; Chhowalla, M. Photoluminescence from Chemically Exfoliated MoS₂. *Nano Lett.* **2011**, *11*, 5111-5116.
2. Furimsky, E. Role of MoS₂ and WS₂ in Hydrodesulfuritation. *Catal. Rev. -Sci. Eng.* **1980**, *22*, 371-400.
3. Chen, Z. B.; Cummins, D.; Reinecke, B. N.; Clark, E.; Sunkara, M. K.; Jaramillo, T. F. Core-shell MoO₃-MoS₂ Nanowires for Hydrogen Evolution: A Functional Design for Electrocatalytic Materials. *Nano Lett.* **2011**, *11*, 4168-4175.
4. Geim, A. K.; Novoselov, K. S. The rise of graphene. *Nat. Mater.* **2007**, *6*, 183-191.
5. Wu, J. S.; Pisula, W.; Mullen, K. Graphenes as Potential Material for Electronics. *Chem. Rev.* **2007**, *107*, 718-747.
6. Kim, K. S.; Zhao, Y.; Jang, H.; Lee, S. Y.; Kim, J. M.; Ahn, J. H.; Kim, P.; Choi, J. Y.; Hong, B. H. Large-Scale Pattern Growth of Graphene Films for Stretchable Transparent Electrodes. *Nature* **2009**, *457*, 706-710.
7. Balandin, A. A.; Ghosh, S.; Bao, W. Z.; Calizo, I.; Teweldebrhan, D.; Miao, F.; Lau, C. N. Superior Thermal Conductivity of Single-Layer Graphene. *Nano Lett.* **2008**, *8*, 902-907.
8. Stankovich, S.; Dikin, D. A.; Dommett, G. H. B.; Kohlhaas, K. M.; Zimney, E. J.; Stach, E. A.; Piner, R. D.; Nguyen, S. T.; Ruoff, R. S. Graphene-Based Composite Materials. *Nature* **2006**, *442*, 282-286.
9. Geim, A. K. Graphene: Status and Prospects. *Science* **2009**, *324*, 1530-1534.
10. Braga, D.; Lezama, I. G.; Berger, H.; Morpurgo, A. F. Quantitative Determination of the Band Gap of WS₂ with Ambipolar Ionic Liquid-Gated Transistors. *Nano Lett.* **2012**, *12*, 5218-5223.
11. Chianelli, R. R.; Siadati, M. H.; De la Rosa, M. P.; Berhault, G.; Wilcoxon, J. P.; Bearden, R.; Abrams, B. L. Catalytic Properties of Single Layers of Transition Metal Sulfide Catalytic Materials. *Catal. Rev. -Sci. Eng.* **2006**, *48*, 1-41.
12. Li, Y. G.; Wang, H. L.; Xie, L. M.; Liang, Y. Y.; Hong, G. S.; Dai, H. J. MoS₂ Nanoparticles Grown on Graphene: An Advanced Catalyst for the Hydrogen Evolution Reaction. *J. Am. Chem. Soc.* **2011**, *133*, 7296-7299.
13. Radisavljevic, B.; Radenovic, A.; Brivio, J.; Giacometti, V.; Kis, A. Single-Layer MoS₂ Transistors. *Nat. Nanotechnol.* **2011**, *6*, 147-150.
14. Yin, Z. Y.; Li, H.; Jiang, L.; Shi, Y. M.; Sun, Y. H.; Lu, G.; Zhang, Q.; Chen, X. D.; Zhang, H. Single-Layer MoS₂ Phototransistors. *ACS Nano* **2012**, *6*, 74-80.
15. Splendiani, A.; Sun, L.; Zhang, Y. B.; Li, T. S.; Kim, J.; Chim, C. Y.; Galli, G.; Wang, F. Emerging Photoluminescence in Monolayer MoS₂. *Nano Lett.* **2010**, *10*, 1271-1275.

16. Novoselov, K. S.;Jiang, D.;Schedin, F.;Booth, T. J.;Khotkevich, V. V.;Morozov, S. V.;Geim, A. K. Two-Dimensional Atomic Crystals. *Proc. Natl. Acad. Sci. U.S.A.* **2005**, *102*, 10451-10453.
17. Joensen, P.;Frindt, R. F.;Morrison, S. R. Single-Layer MoS₂. *Mater. Res. Bull.* **1986**, *21*, 457-461.
18. Korn, T.;Heydrich, S.;Hirmer, M.;Schmutzler, J.;Schuller, C. Low-Temperature Photocarrier Dynamics in Monolayer MoS₂. *Appl. Phys. Lett.* **2011**, *99*, 102109.
19. Li, T. S.;Galli, G. L. Electronic Properties of MoS₂ Nanoparticles. *J. Phys. Chem. C* **2007**, *111*, 16192-16196.
20. Mak, K. F.;Lee, C.;Hone, J.;Shan, J.;Heinz, T. F. Atomically Thin MoS₂: A New Direct-Gap Semiconductor. *Phys. Rev. Lett.* **2010**, *105*, 136805
21. Lee, H. S.;Min, S. W.;Chang, Y. G.;Park, M. K.;Nam, T.;Kim, H.;Kim, J. H.;Ryu, S.;Im, S. MoS₂ Nanosheet Phototransistors with Thickness-Modulated Optical Energy Gap. *Nano Lett.* **2012**, *12*, 3695-3700.
22. Coleman, J. N.;Lotya, M.;O'Neill, A.;Bergin, S. D.;King, P. J.;Khan, U.;Young, K.;Gaucher, A.;De, S.;Smith, R. J.;Shvets, I. V.;Arora, S. K.;Stanton, G.;Kim, H. Y.;Lee, K.;Kim, G. T.;Duesberg, G. S.;Hallam, T.;Boland, J. J.;Wang, J. J.;Donegan, J. F.;Grunlan, J. C.;Moriarty, G.;Shmeliov, A.;Nicholls, R. J.;Perkins, J. M.;Grieverson, E. M.;Theuwissen, K.;McComb, D. W.;Nellist, P. D.;Nicolosi, V. Two-Dimensional Nanosheets Produced by Liquid Exfoliation of Layered Materials. *Science* **2011**, *331*, 568-571.
23. Hong, J.;Han, J. Y.;Yoon, H.;Joo, P.;Lee, T.;Seo, E.;Char, K.;Kim, B. S. Carbon-Based Layer-by-Layer Nanostructures: From Films to Hollow Capsules. *Nanoscale* **2011**, *3*, 4515-4531.
24. Osada, M.;Sasaki, T. Two-Dimensional Dielectric Nanosheets: Novel Nanoelectronics From Nanocrystal Building Blocks. *Adv. Mater.* **2012**, *24*, 210-228.
25. Ollivier, P. J.;Kovtyukhova, N. I.;Keller, S. W.;Mallouk, T. E. Self-Assembled Thin Films from Lamellar Metal Disulfides and Organic Polymers. *Chem. Comm.* **1998**, 1563-1564.
26. Liu, K. K.;Zhang, W. J.;Lee, Y. H.;Lin, Y. C.;Chang, M. T.;Su, C.;Chang, C. S.;Li, H.;Shi, Y. M.;Zhang, H.;Lai, C. S.;Li, L. J. Growth of Large-Area and Highly Crystalline MoS₂ Thin Layers on Insulating Substrates. *Nano Lett.* **2012**, *12*, 1538-1544.
27. Yang, D.;Sandoval, S. J.;Divigalpitiya, W. M. R.;Irwin, J. C.;Frindt, R. F. Structure of Single Molecular Layer MoS₂. *Phys. Rev. B* **1991**, *43*, 12053-12056.
28. Py, M. A.;Haering, R. R. Structural Destabilization Induced by Lithium Intercalation in MoS₂ and Related-Compounds. *Can. J. Phys.* **1983**, *61*, 76-84.
29. Liu, C. J.;Tai, S. Y.;Chou, S. W.;Yu, Y. C.;Chang, K. D.;Wang, S.;Chien, F. S. S.;Lin, J. Y.;Lin, T. W. Facile Synthesis of MoS₂/Graphene Nanocomposite with High Catalytic Activity toward Triiodide Reduction in Dye-Sensitized Solar Cells. *J. Mater. Chem.* **2012**, *22*, 21057-

21064.

30. Lee, C.; Yan, H.; Brus, L. E.; Heinz, T. F.; Hone, J.; Ryu, S. Anomalous Lattice Vibrations of Single- and Few-Layer MoS₂. *ACS Nano* **2010**, *4*, 2695-2700.

Acknowledgement

저를 낳아주시고 부족함 없이 키워주신 아버지, 어머니께 이 논문을 바칩니다. 사춘기 무렵 공부는 안하고 매일 빈둥대고 놀기만 하는 아들을 보면서 많이 답답하셨을 모습을 생각하면 너무 죄송스럽습니다. 늦었지만 앞으로는 항상 진취적인 사고를 가지고 자신을 채찍질 하면서 도태되지 않도록 노력하고 잘 되는 모습만 보여드리도록 노력 하겠습니다.

2년 동안 부족한 저에게 많은 가르침을 주신 지도 교수님이신 김병수 교수님께 깊은 감사를 드립니다. 신생학교인 UNIST에서 2년간 많은 고생을 한 만큼 얻어가는 것도 많기 때문에 인생에서 큰 도움이 되리라고 생각 됩니다. 처음 오픈 랩에 참가를 하여 함께 시작한 수은이, 랩의 첫 학생으로 너무 고생을 많이 한 태민이, 항상 힘들 때 옆에서 도움이 되어준 은용이 형, 그리고 유리, 은경이, 은희에게 고맙다는 말을 전해주고 싶습니다. 그리고 항상 밤늦도록 같이 실험을 도와주었던 학부생 국문이, 응진이, 그리고 기영이에게 너무 고맙고 앞으로 대학원에 입학해서 더욱 깊이 있는 연구를 하여 학교와 연구실을 빛낼 수 있는 학생이 되도록 옆에서 응원을 하겠습니다.

처음에 연구를 시작하여 아무것도 모를 때 많은 것을 가르쳐준 동욱이 형, 그리고 학부시절부터 많은 아이디어를 공유한 범준이 에게도 항상 고마운 마음을 가지고 있습니다. 학부시절 지도교수이자 공동연구를 진행 해 주신 조정호 교수님께도 깊은 감사를 드립니다. 지난 여름 World Class University 프로그램을 통해 방문연구를 진행 하면서 많은 도움을 준 Damien, Raj, Muharrem, Mariam, 그리고 Manish 교수님께도 감사를 드리고 싶습니다.

짧다면 짧고 길다면 긴 2년이라는 시간 동안 정말 많이 배웠습니다. 처음에 연구실 생활을 하면서 막연하게 논문을 읽고 별 생각 없이 실험을 하면서 지치기도 했고, 많은 시간을 낭비했습니다. 하지만 시간이 지나면서 일이 손에 익어가고 문제를 해결 해 나가는 힘을 키우면서 가장 중요한 것을 깨달았습니다. 아주 오래된 고전논문을 참고하여 차근 차근 논리적으로 일을 맞추어 나가면 시간을 낭비하는 일이 많지 않고, 항상 생각을 하면서 실험을 해야 해결책을 찾아 낼 수 있었습니다. 가끔씩 지난 주간보고서들을 보면서 자신이 부끄러워 질 때가 있습니다. ‘정말 이렇게 밖에 못했나? 이걸 뭐지?’ 라는 생각이 들곤 합니다. 하지만 이러한 시행착오들이 있었기 때문에 더욱 발전을 할 수 있었다고 생각합니다. 제가 교수님 입장에서 저 같은 학생을 가르쳤으면 구타를 했을지도 모르겠다는 생각을 가끔 합니다. 교수님께서 까칠하고 부족한 저를 가르치시느라 고생이 참 많으셨습니다. 사회에 나가서도 KBS group에서 배운 것을 토대로 열심히 하기도 하지만 일

을 잘 하는 사람으로 인정받도록 하겠습니다.

다른 연구실에 비해서 우리 연구실이 타이트하게 진행되는 것은 맞는 것 같습니다. 주말 랩 미팅, 많은 연구과제, 주말까지 무언가 만들어야 한다는 압박 등등... 2년간 상당한 압박에 쉽지 않은 생활을 했다고 생각을 하지만, 지금 돌이켜 보면 이렇게 했기 때문에 얻어가는 것이 상당히 많았다고 생각 합니다. KBS group 학생들 모두 조금만 더 힘내면 빛나는 연구성과를 낼 수 있습니다. 항상 노력합시다. 파이팅!~